REPORT DOCUMENTATION PAGE

Form Approved
OMB NO. 0704-0188

Public Reporting burden for this collection of information is estimated to average 1 hour per response, including the time for reviewing instructions, searching existing data sources, gathering and maintaining the data needed, and completing and reviewing the collection of information. Send comment regarding this burden estimates or any other aspect of this collection of information, including suggestions for reducing this burden, to Washington Headquarters Services, Directorate for information Operations and Reports, 1215 Jefferson Davis Highway, Suite 1204, Arlington, VA 22202-4302, and to the Office of Management and Budget, Paperwork Reduction Project (0704-0188.) Washington, DC 20503.

1. AGENCY USE ONLY (Leave Blank)	2. REPORT DATE	3. REPORT TYPE AND DATES COVERED
	August 21, 2000	Final Progress Report,

4. TITLE AND SUBTITLE
Use of Aeroelastic Couplings and Multi-Point Optimization to Design Damperless Aeromechanically Stable Helicopters

5. FUNDING NUMBERS
DAAG55-97-1-0347

6. AUTHOR(S)
Dr. Farhan Gandhi

7. PERFORMING ORGANIZATION NAME(S) AND ADDRESS(ES)
Dr. Farhan Gandhi
Department of Aerospace Engineering, The Pennsylvania Sate University
233 Hammond Building, University Park, PA 16802

8. PERFORMING ORGANIZATION REPORT NUMBER

9. SPONSORING / MONITORING AGENCY NAME(S) AND ADDRESS(ES)
U. S. Army Research Office
P.O. Box 12211
Research Triangle Park, NC 27709-2211

10. SPONSORING / MONITORING AGENCY REPORT NUMBER
ARO 35828.3-EG-Y/P

11. SUPPLEMENTARY NOTES
The views, opinions and/or findings contained in this report are those of the author(s) and should not be construed as an official Department of the Army position, policy or decision, unless so designated by other documentation.

12 a. DISTRIBUTION / AVAILABILITY STATEMENT
Approved for public release; distribution unlimited.

12 b. DISTRIBUTION CODE

13. ABSTRACT (Maximum 200 words)

The present study examines the effectiveness of optimized aeroelastic couplings and rotor stiffness properties for improving the aeromechanical stability characteristics of a helicopter with a soft-inplane rotor, over a wide range of conditions, to enable the elimination of auxiliary lag dampers. A refined optimization procedure is developed that is robust and numerically efficient. Using this procedure, results indicate that it is possible to significantly reduce the peak instability levels, while enforcing constraints on design variables, and the rotating flap and lag frequencies. Concurrent optimization of the aeroelastic couplings and rotor stiffness parameters, rather than a sequential optimization strategy, yielded a design which provided maximum improvement in aeromechanical stability characteristics. The optimized design for the ground contact condition also resulted in improved lag damping in hover and forward flight. By appropriately selecting additional design parameters such as landing gear stiffness and damping it is possible to altogether alleviate instabilities in the optimized design.

20001124 033

14. SUBJECT TERMS
aeromechanical stability, aeroelastic couplings, optimization
ground resonance and air resonance
damperless helicopter rotors

15. NUMBER OF PAGES

16. PRICE CODE

17. SECURITY CLASSIFICATION OR REPORT	18. SECURITY CLASSIFICATION ON THIS PAGE	19. SECURITY CLASSIFICATION OF ABSTRACT	20. LIMITATION OF ABSTRACT
UNCLASSIFIED	UNCLASSIFIED	UNCLASSIFIED	UL

DTIC QUALITY INSPECTED 4

USE OF AEROELASTIC COUPLINGS AND MULTI-POINT OPTIMIZATION TO DESIGN DAMPERLESS AEROMECHANICALLY STABLE HELICOPTERS

FINAL PROGRESS REPORT

FARHAN GANDHI

ERIC HATHAWAY

AUGUST 21, 2000

U.S. ARMY RESEARCH OFFICE

35828-EG

PENNSYLVANIA STATE UNIVERSITY

APPROVED FOR PUBLIC RELEASE;

DISTRIBUTION UNLIMITED

THE VIEWS, OPINIONS, AND/OR FINDINGS CONTAINED IN THIS REPORT ARE THOSE OF THE AUTHOR(S) AND SHOULD NOT BE CONSTRUED AS AN OFFICIAL DEPARTMENT OF THE ARMY POSITION, POLICY, OR DECISION, UNLESS SO DESIGNATED BY OTHER DOCUMENTATION.

Foreword

The present study examines the effectiveness of optimized aeroelastic couplings and rotor stiffness properties for improving the aeromechanical stability characteristics of a helicopter with a soft-inplane rotor, over a wide range of conditions, to enable the elimination of auxiliary lag dampers. A refined optimization procedure is developed that is robust and numerically efficient. Using this procedure, results indicate that it is possible to significantly reduce the peak instability levels, while enforcing constraints on design variables, and the rotating flap and lag frequencies. Concurrent optimization of the aeroelastic couplings and rotor stiffness parameters, rather than a sequential optimization strategy, yielded a design which provided maximum improvement in aeromechanical stability characteristics. The optimized design for the ground contact condition also resulted in improved lag damping in hover and forward flight. By appropriately selecting additional design parameters such as landing gear stiffness and damping it is possible to altogether alleviate instabilities in the optimized design.

Table of Contents

List of Figures

USE OF AEROELASTIC COUPLINGS AND MULTI-POINT OPTIMIZATION TO DESIGN DAMPERLESS AEROMECHANICALLY STABLE HELICOPTERS

Introduction

Helicopters with soft-inplane rotors are susceptible to aeromechanical instabilities due to the interaction of the poorly damped regressing lag mode and the body modes [1]. Traditionally, such helicopters have been equipped with auxiliary lead-lag dampers to alleviate aeromechanical instability. However, associated with the use of lag dampers are issues such as hub complexity, weight, aerodynamic drag, and maintenance requirements. Modern day elastomeric dampers are also expensive, susceptible to fatigue, and exhibit complex nonlinear behaviors. Further, elastomeric dampers are sensitive to temperature, exhibiting significant loss of damping at very high or very low temperatures, and have been known to cause limit cycle oscillations in rotor blades. As a result of these factors, a variety of alternatives to auxiliary lag dampers are under consideration. The elimination of lag dampers would further simplify the hub, and reduce weight, aerodynamic drag, and maintenance costs. However, the design of a damperless, yet aeromechanically stable, configuration is truly a challenge [2,3]. While several concepts have shown promise, there has been no generally accepted solution for eliminating lag dampers.

One alternative to auxiliary lag dampers for the provision of adequate aeromechanical stability margins is the use of aeroelastic couplings. Numerous studies [4–15] have demonstrated the potential of aeroelastic couplings for increasing lag mode damping. The most noteworthy investigations of the effects of aeroelastic couplings on helicopter aeromechanical stability were conducted at the Army Aeroflightdynamics Directorate at Ames. Initial investigations, begun over twenty years ago, examined the effects of pitch-lag and flap-lag couplings on an isolated hingeless rotor [4-6]. These studies indicated that a combination of these couplings was effective in increasing rotor lag damping. Further studies expanded the investigation to examine the effects of aeroelastic couplings on the coupled rotor-body aeromechanical stability of a hingeless rotor [7-9]. It was found that combinations of aeroelastic couplings were beneficial for the aeromechanical stability characteristics, particularly at higher values of collective pitch.

Other work in this area [10-14] has examined the effects of aeroelastic couplings on aeromechanical stability characteristics under various operating conditions. All of these investigations have primarily focused on parametric studies of stability trends, examining discrete values of the coupling parameters at a limited number of operating conditions.

For aeroelastic couplings to be used as a practical alternative to auxiliary lag dampers, they must be able to provide acceptable levels of stability over a wide range of operating conditions (i.e. variations in thrust level, variations in body inertia, ground contact as well as airborne condition). This is a challenge, because different operating conditions often have conflicting requirements for stability augmentation. For example, a value of pitch-flap coupling having a stabilizing influence at a flat pitch condition may be destabilizing at a high thrust condition. One strategy for the determination of favorable values of aeroelastic couplings, investigated in [15], used formal optimization techniques to address these conflicting stability requirements and identify a unique combination of aeroelastic coupling parameters that significantly augmented lag mode damping over a broad range of operating conditions.

While aeroelastic couplings can positively influence aeromechanical stability, they also have a significant effect on the rotor frequencies, particularly flap frequency. Values of aeroelastic couplings that are generally stabilizing for ground resonance may result in rotor frequencies that are unacceptable from a handling qualities perspective. The other fundamental parameters in determining flap and lag frequencies are the blade flap and lag stiffnesses. In addition to aeroelastic couplings, these stiffness parameters are introduced as design variables in the present study. The optimization techniques of Ref. [15] are significantly improved, yielding a faster and more numerically robust procedure. The goal of the expanded optimization procedure in the present study is to retain the stabilizing influence of aeroelastic couplings, while using the added design flexibility offered by the inclusion of rotor stiffness properties (as design parameters) to enforce constraints which will prevent excessively large changes in rotor frequencies. It will be shown that this *concurrent optimization* approach, where the aeroelastic couplings and fundamental rotor stiffness parameters are simultaneously considered as design parameters, is superior to a *sequential* approach where blade stiffness and frequency targets are set prior to any attempt to incorporate aeroelastic couplings. The concurrent optimization approach provides better performance (increased stability levels), while at the same time satisfying imposed frequency constraints. The aeromechanical stability characteristics of concurrently optimized designs will be examined for variations in body inertia, and operating condition (including ground contact, hover, and forward flight) to demonstrate the robustness of the optimized design. Furthermore, it will be shown that by using a combination of parameters (optimized aeroelastic couplings and rotor stiffness properties, together with landing gear stiffness and damping properties), it is possible to provide adequate aeromechanical stability margins without the use of an auxiliary lag damper.

Rotor-Fuselage Analytical Model

The analytical model used in the present study represents a three-bladed rotor whose blades have uniform mass distribution and are assumed to undergo rigid flap rotations (β) and lag rotations (ζ) about spring-restrained offset hinges. The fuselage is assumed to undergo rigid body roll and pitch rotations (α_x and α_y) about its center of mass (located directly below the hub). The aerodynamic loads on the rotor blades are calculated using quasi-steady strip theory, assuming a uniform inflow.

The rotor-fuselage equations of motion are linearized about the equilibrium condition to obtain the perturbation equations. The perturbation flap and lag equations for the individual blades (having periodic coefficients in the rotating coordinate system) are transformed to the non-rotating coordinate system using Multiblade Coordinate Transforms. For ground contact or hover conditions, this transformation yields a collective equation and two cyclic equations in the non-rotating system for flap and lag motions, all of which have constant coefficients (independent of azimuthal position of the blade). The two cyclic flap and cyclic lag equations couple with the fuselage motions, and thus need to be retained for the aeromechanical stability analysis. In addition, the collective flap and collective lag equations are retained and used to track the rotating flap and lag frequencies. Thus, the rotor-fuselage model for a three-bladed rotor has eight degrees of freedom: collective flap (β_o), cyclic flap (β_{1c} and β_{1s}), collective lag (ζ_o), cyclic lag (ζ_{1c} and ζ_{1s}), and fuselage roll and pitch (α_x and α_y). In the non-rotating frame the resulting constant coefficient system can be represented in the following form:

$$[M]\{\ddot{q}\}+[C]\{\dot{q}\}+[K]\{q\}=\{0\} \tag{1}$$

where [M], [C], and [K] are the 8 x 8 mass, damping and stiffness matrices, and

$$\{q\}=\lfloor \beta_o \quad \beta_{1c} \quad \beta_{1s} \quad \zeta_o \quad \zeta_{1c} \quad \zeta_{1s} \quad \alpha_x \quad \alpha_y \rfloor^T \tag{2}$$

The eigenvalues of Eq. 1 yield the modal frequencies and decay rates.

The aeroelastic coupling parameters considered (and contained in Eq.1 are: pitch-flap coupling ($K_{P\beta}$), pitch-lag coupling ($K_{P\zeta}$), and structural flap-lag coupling (R_β and R_ζ).

The pitch-flap and pitch-lag couplings result in perturbations in blade pitch, $\Delta\theta$, due to perturbation flap and lag motions. Thus,

$$\Delta\theta_k = -K_{P\beta}\beta_k - K_{P\zeta}\zeta_k \tag{3}$$

where the subscript "k" denotes the k^{th} blade. Careful attention should be paid to sign convention here. In the present model, β is positive for flap-up motion, ζ is positive for lag-back, and $\Delta\theta$ is positive for nose-up pitching motion. Thus, a positive value of $K_{P\beta}$ would result in a flap-up, pitch nose-down coupling, while a positive $K_{P\zeta}$ would yield a lag-back, pitch nose-down coupling.

Structural flap-lag coupling is a result of blade flap and lag flexibility outboard of the pitch bearing. In Ref. [16] flap-lag coupling was modeled using orthogonal hub flap and lag springs $k_{\beta H}$ and $k_{\zeta H}$, respectively, inboard of the pitch bearing; and orthogonal blade flap and lag springs $k_{\beta B}$ and $k_{\zeta B}$, respectively, outboard of the pitch bearing. Based on this system of springs, effective flap and lag flexural stiffnesses k_β and k_ζ were defined as

$$k_\beta = \frac{k_{\beta H}k_{\beta B}}{k_{\beta H}+k_{\beta B}} \qquad\qquad k_\zeta = \frac{k_{\zeta H}k_{\zeta B}}{k_{\zeta H}+k_{\zeta B}} \tag{4}$$

Structural flap-lag coupling parameters are then defined as

$$R_\beta = k_\beta/k_{\beta B} \qquad\qquad R_\zeta = k_\zeta/k_{\zeta B} \tag{5}$$

where, for example, $R_\beta = 1$, means the flap flexibility is entirely outboard of the pitch bearing with the hub being rigid in flap, and $R_\beta = 0$, means the flap flexibility is entirely in the hub with the region outboard of the pitch bearing being rigid in flap. In general, if there is some flexibility in both the hub and the blade, R_β and R_ζ assume values between 0 and 1. A complete formulation of the structural flap-lag coupling parameters is found in Ref. [15].

Blade stiffness parameters are defined to allow variations about the nominal flap and lag stiffnesses, $\overline{K}_\beta$ and $\overline{K}_\zeta$, respectively. Thus,

$$\begin{aligned} K_\beta &= \overline{K}_\beta\left(1+\Delta K_\beta\right) \\ K_\zeta &= \overline{K}_\zeta\left(1+\Delta K_\zeta\right) \end{aligned} \tag{6}$$

where ΔK_β and ΔK_ζ are non-dimensional design parameters representative of a percent change in stiffness about the baseline values.

Validation of Analytical Model

The analytical model is validated using the experimental results in Ref. [8]. Rotor-fuselage properties for this configuration are given in Table 1. Figure 1 shows the variation in regressing lag damping, body pitch damping, and body roll damping, for 0° collective. It is seen that the regressing lag damping, as well as body pitch and roll damping compare very well with experiment.

Figures 2 and 3 show the variation of regressing lag mode damping versus rotational speed at 9° collective for the cases of no aeroelastic coupling, and for a pitch-lag coupling, $K_{P\zeta} = -0.4$, respectively. Once again, in both cases, the analytical predictions compare well with experimental results.

Finally, Figure 4 show variations of regressing lag damping versus collective pitch at rotational speeds of 760 and 820 RPM. Again, the analytical results compare very well with experiment.

Extension of Analysis to Forward Flight

The aeromechanical stability analysis described above is extended to the forward flight condition. For this case, the periodic coefficients of the equations are not eliminated even after transforming to the non-rotating system. Thus, the matrices are functions of blade azimuthal position, and the system can be represented as:

$$[M]\{\ddot{q}\}+[C(\psi)]\{\dot{q}\}+[K(\psi)]\{q\}=\{0\} \tag{7}$$

The eigenvalues of the above equations can be obtained using either the Floquet Transition Matrix theory or a constant coefficient approximation. In the second approach, the matrices are numerically evaluated at a prescribed number of points around the rotor azimuth and simply averaged. The eigenvalues of the resulting constant coefficient equations then yield the rotor-body frequency and damping characteristics in forward flight.

The constant coefficient approximation technique, which is much simpler than the Floquet Transition matrix approach, has been shown to be accurate (see Ref. [17]), and is used in the present study to evaluate aeromechanical stability characteristics in forward flight.

Steady Inflow vs. Dynamic Inflow

As mentioned previously, the present analysis uses a uniform inflow model to determine the aerodynamic loads on the rotor blades. It has been suggested that accurate prediction of helicopter aeromechanical stability characteristics requires the inclusion of a dynamic inflow model. However, this is not necessarily the case. Figures 5-6 compare the lag mode stability characteristics of both a baseline (no couplings) configuration and a configuration with optimized aeroelastic couplings (from Ref. [15]), using both a steady inflow model and a dynamic inflow model. Figure 5 shows that at a collective pitch of 5 degrees, dynamic inflow has an insignificant effect on lag damping for both the baseline and optimized configuration. From figure 6 (a plot of the *minimum* damping, corresponding to the bottom of the resonance bucket, versus collective pitch) it is seen that this observation holds true over the entire range of collective pitch values under consideration.

Dynamic inflow is known to have a significant effect on the damping of body modes, but has a much smaller effect on lag mode damping. Further, while dynamic inflow may affect the specific damping level for a particular configuration at a given operating condition, it does not affect the overall stability trends with variations in rotor speed, collective pitch, or aeroelastic coupling parameters. Since the present study is an investigation into the effects that aeroelastic couplings have on lag mode stability trends, rather than a rigorous calculation of aeromechanical stability levels for a specific full-scale design effort, dynamic inflow has not been included in the subsequent results.

Influence of Individual Design Variables

Before conducting any optimization studies, it is useful to develop an understanding of the individual influence of each design variable on aeromechanical stability. The baseline rotor configuration used for the numerical studies in this paper is a model hingeless rotor tested at NASA-Ames [7], whose properties are given in Table 1. This baseline configuration has no aeroelastic couplings (i.e. $K_{P\beta}$, $K_{P\zeta}$, R_β, $R_\zeta = 0$).

Influence of Pitch-Flap Coupling on Aeromechanical Stability

In Figure 7 it is seen that for 5° collective pitch, positive pitch-flap coupling (flap up - nose down) is able to increase the minimum damping at resonance conditions. The results in Figure 7 indicate that the increase in minimum damping is a nonlinear function of degree of positive pitch-flap coupling. After obtaining a significant increase in minimum damping for small values of pitch-flap coupling, further increases in pitch-flap coupling result in smaller additional increases in minimum damping.

Figure 8 shows that this increase in the level of minimum damping is found at all values of collective pitch, though the degree of stabilization is increased at high collective. Examination of plots similar to Figure 8 for other values of pitch-flap coupling indicates that the trend of smaller increases in minimum damping as $K_{P\beta}$ becomes larger holds true for all values of collective pitch.

Influence of Pitch-Lag Coupling on Aeromechanical Stability

Figure 9 shows the influence of negative pitch-lag coupling (lag back - nose up) on lag damping in ground resonance at 5° collective pitch. It is seen that while there is no change in the minimum damping values at resonance, negative pitch-lag coupling increases the damping away from resonance. The net effect is that the range of rotational speeds over which instability is encountered can be significantly reduced.

Figure 10 shows that effect of negative pitch-lag coupling varies greatly with collective pitch. Above 5° collective, negative $K_{P\zeta}$ is seen to be quite stabilizing, whereas below 5° collective, it is destabilizing. Examining plots similar to Figure 9 at lower values of collective pitch shows that this destabilizing effect is happening in the resonance region. Away from resonance, negative pitch-lag coupling is stabilizing for all values of collective pitch.

In Figures 7 and 9 it is seen that both negative pitch-lag coupling as well as positive pitch-flap coupling tend to shift the resonance condition to a slightly lower rotational speed.

Influence of Structural Flap-Lag Coupling on Aeromechanical Stability

Figure 11 shows that structural flap-lag couplings are unable to increase the minimum damping at roll resonance. Of the two parameters, R_β and R_ζ, regressing lag damping is more sensitive to changes in R_β. The regressing lag damping with $R_\zeta = 1$ is almost identical to the baseline. For the case $R_\beta = R_\zeta = 1$ (results not shown in Figure 11), the regressing lag damping was found to be almost identical to the case $R_\beta = 1$, $R_\zeta = 0$. It should be mentioned that structural flap-lag coupling would have a larger influence at higher values of collective pitch.

Influence of Blade Flap Stiffness on Aeromechanical Stability

Figure 12 shows the influence of rotor blade flap stiffness on ground resonance stability. Increasing the flap stiffness is seen to have a mild stabilizing effect. In Figure 13 it is seen that this trend holds true for

all values of collective pitch, with the degree of stabilization increasing at high collective pitch. This is consistent with the findings in [7], where increased flap stiffness was shown to have a beneficial influence on stability boundaries for blade lead-lag frequencies greater than approximately 0.6 (as is the case with the present model). Figure 14 shows that this stabilizing trend with increased flap stiffness continues for the hover condition (however, at the nominal speed of the rotor of 720 RPM, the increase in stability is insignificant). In the present study all "hover" results are obtained by setting the fuselage pitch and roll spring stiffnesses to zero and trimming the rotor to a constant (non-zero) thrust. It can also be seen in Figures 12 and 14 that the rotational speed at which resonance occurs is unchanged. These results would seem to contradict the findings in [7], where increased flap frequency was found to destabilize air resonance. However, the air resonance results in [7] were for a flat pitch condition, whereas the present air resonance analysis trimmed collective pitch to produe a constant thrust. Thus, direct comparisons between the two studies may not be appropriate.

Although increased flap stiffness has an overall positive influence on ground and air resonance stability, it should be noted that blade flap stiffness cannot be increased arbitrarily. Other concerns, such as dynamic stresses in the flap flexure, set an upper limit on the level of flap stiffness that can be realized in practice.

Influence of Blade Lag Stiffness on Aeromechanical Stability

Figure 15 shows the influence of rotor blade lag stiffness on ground resonance stability. Increasing lag stiffness reduces the level of instability slightly, while also shifting the maximum instability to a higher rotational speed. This shift in the rotational speed at which resonance occurs is expected, because increasing the rotor lag stiffness will cause the regressing lag mode to coalesce with the body modes at a higher rotational speed, delaying the onset of aeromechanical instabilities. This is again consistent with the results reported in [7], where increased lag frequencies generally improved stability boundaries. In Figure 16, it can be seen that as collective pitch is increased, the degree of stabilizing influence from increased lag stiffness decreases, and at very high pitch settings, increased lag stiffness can actually be destabilizing. Figure 17 shows that for the hover condition, increasing lag stiffness again shifts the instability to a higher rotational speed, and this can potentially lower air resonance stability margins at the nominal speed (720 RPM). In addition, excessively large values of lag stiffness would produce unacceptable dynamic stress levels in the blade flexure.

Parametric Optimization

Formal optimization procedures were used with the goal of determining a combination of the design variables that will alleviate aeromechanical instabilities, while constraining flap and lag frequencies within prescribed values. The design variables considered were rotor pitch-flap coupling parameter ($K_{P\beta}$), pitch-lag coupling parameter ($K_{P\zeta}$), structural flap-lag coupling parameters (R_β and R_ζ), as well as changes in blade flap stiffness (ΔK_β) and lag stiffness (ΔK_ζ).

Parametric design optimization is implemented using the subroutine DNCONF, from the IMSL mathematical library subroutines. This is a gradient-based optimizer which uses a successive quadratic programming algorithm to solve the general nonlinear programming problem with nonlinear constraints. The user of this subroutine is required to define a set of design variables, as well as provide a routine which evaluates some objective function. The optimizer then seeks to find the combination of design variables such that the objective function is minimized. Gradients are calculated numerically for each iteration to determine the search direction, using a finite difference method.

The objective function must be selected thoughtfully, in order to achieve the desired results. In the present study, a number of objective functions are formulated before satisfactory results are achieved. These successive formulations are presented here, along with discussions of intermediate results, to provide insight into the subtleties involved in successfully formulating this design optimization problem.

Single-Point Optimization

Design optimization is initially carried out at a moderate thrust condition (collective pitch of 5°). Since the baseline system (without any aeroelastic couplings) reaches minimum damping at about 770 RPM, the objective function to be minimized is defined as follows:

$$F(D_j) = (\sigma_{770} - \bar{\sigma}_{770})^2 \tag{8}$$

where σ_{770} denotes the regressing lag mode decay rate at 770 RPM, $\bar{\sigma}_{770}$ denotes the desired regressing lag mode decay rate at 770 RPM (which was set at -0.1, stable), and D_j denotes the j^{th} design variable.

The following constraints are imposed on the design variables:

$$-1.0 \le K_{P\beta} \le 1.0 \qquad -1.0 \le K_{P\zeta} \le 1.0$$
$$0.0 \le R_{\beta} \le 1.0 \qquad 0.0 \le R_{\zeta} \le 1.0 \tag{9}$$

The sensitivity gradients, $\frac{\partial \sigma_{770}}{\partial D_j}$, required in the optimization procedure, are calculated numerically by perturbing the individual design variables. The optimization procedure yielded the following results:

$$K_{P\beta} = 0.328 \qquad K_{P\zeta} = -0.448$$
$$R_{\beta} = 0.997 \qquad R_{\zeta} = 0.998 \tag{10}$$

Figure 18 shows the variation of regressing lag damping versus rotational speed when these optimal values of aeroelastic couplings are used. It is interesting to note that satisfaction of the objective function ($\sigma_{770} = \overline{\sigma}_{770}$) is accomplished by moving the resonance condition to a lower rotational speed. The net result is that although increase in regressing lag damping is obtained over the baseline, instability of the regressing lag mode is still present. Similar results were obtained for increasing values of $\overline{\sigma}_{770}$, i.e., resonance moved to a lower rotational speed and instability persisted.

Of the "optimized" aeroelastic coupling parameters, the structural flap-lag couplings do not have a major influence. The initial guess for R_{β} and R_{ζ} was 1, and the optimized values remained close to the initial guess. When the initial guess was selected at zero, the optimizer yielded virtually the same values of $K_{P\beta}$ and $K_{P\zeta}$, but the values of R_{β} and R_{ζ} remained close to zero. Even in the latter case (R_{β}, $R_{\zeta} \approx 0$), the aeromechanical stability characteristics were very similar to the "optimized" results presented in Figure 18.

Single-Point Optimization with Multi-Point Constraints

It was seen that the single-point optimization procedure was effective in producing the desired level of damping at the specified rotational speed (770 RPM), but this was achieved only by moving the resonance condition to another rotational speed. In order to improve aeromechanical stability over a wide range of rotational speeds, and to prevent satisfaction of the objective function merely by moving the resonance to a different rotational speed, stability constraints are introduced at a number of rotational speeds. This time the objective function to be minimized is

$$F(D_j) = (\sigma_{775} - \overline{\sigma}_{775})^2 \tag{11}$$

subject to the following inequality constraints

$$\begin{aligned} g_1(D_j) &= \sigma_{725} \le 0 & g_2(D_j) &= \sigma_{750} \le 0 \\ g_3(D_j) &= \sigma_{800} \le 0 & g_4(D_j) &= \sigma_{825} \le 0 \end{aligned} \tag{12}$$

in addition to constraints on the design variables (Eq. 9).

For this problem, sensitivity gradients at each of the rotational speeds - $\frac{\partial \sigma_{725}}{\partial D_j}$, $\frac{\partial \sigma_{750}}{\partial D_j}$, $\frac{\partial \sigma_{775}}{\partial D_j}$, $\frac{\partial \sigma_{800}}{\partial D_j}$, and $\frac{\partial \sigma_{825}}{\partial D_j}$ - need to be calculated. This requires that each design variable be perturbed at each of the rotational speeds considered. The present optimization procedure yielded the following results (at 5° collective pitch)

$$\begin{aligned} K_{P\beta} &= 0.622 & K_{P\zeta} &= -0.641 \\ R_\beta &= 0.983 & R_\zeta &= 1.0 \end{aligned} \tag{13}$$

Figure 18 also shows the variation of regressing lag damping versus rotational speed when these "optimal" values of aeroelastic couplings are used. The level of instability as well as the RPM range of instability are both reduced as compared to the single-point optimization results, and considerable increase in regressing lag damping is obtained over the baseline. However, the system is not totally stabilized, and the inequality constraint g_1 (Eq. 12), is violated.

Moving-Point Optimization

To completely eliminate the possibility that an objective function at a prescribed rotational speed is satisfied by moving the resonance to a different rotational speed, a moving-point optimization procedure is formulated. The objective function to be minimized is:

$$F(D_j) = (\sigma_{min} - \overline{\sigma}_{min})^2 \tag{14}$$

subject to constraints on the design variables, Eq. 9. In this objective function, σ_{min} denotes the minimum decay rate (which occurs at different rotational speeds as the values of aeroelastic coupling parameters change during the course of the optimization process), and $\bar{\sigma}_{min}$ denotes the desired minimum decay rate. In this procedure, during each iteration in the optimization process, the rotational speed at which the damping is a minimum is determined, and the optimizer then seeks to stabilize the regressing lag mode at this rotational speed. Thus, there is no possibility that an objective function at a prescribed rotational speed will be satisfied by moving resonance to another rotational speed.

The moving-point optimization procedure yielded the following results (at 5° collective)

$$\begin{aligned} K_{P\beta} &\approx 0.6 & K_{P\zeta} &= -1.0 \\ R_{\beta} &= 1.0 & R_{\zeta} &= 0.0 \end{aligned} \tag{15}$$

Figure 19 shows the variation of regressing lag damping versus rotational speed when these optimal values of aeroelastic couplings are used. It is seen that this configuration stabilizes the regressing lag mode over the entire range of rotational speeds.

Next, it must be verified whether these optimal couplings (determined through a moving-point optimization procedure at 5° collective) are effective at different blade pitch settings. Figure 20 shows the variation of regressing lag damping versus rotational speed at 0° collective pitch, obtained using the optimized aeroelastic couplings in Eq. 15. It is seen that "optimal" couplings at 5° collective seriously degrade the stability at 0° collective (as compared to the baseline, with no aeroelastic couplings). Examination of similar plots (regressing lag damping versus rotational speed) at different values of collective pitch showed that the aeroelastic couplings obtained through moving-point optimization at 5°, (Eq. 15), are stabilizing at moderate to high collective pitch settings, but are destabilizing for low collective pitch settings close to 0°.

A moving-point optimization carried out at 0° collective pitch yielded the following optimal aeroelastic couplings:

$$\begin{aligned} K_{P\beta} &= -1.0 & K_{P\zeta} &= 0.07226 \\ R_{\beta} &= 0.0 & R_{\zeta} &= 0.0 \end{aligned} \tag{16}$$

It is seen in Figure 21 that while the above couplings eliminate aeromechanical instability at 0° collective, they are very strongly destabilizing at increasing collective pitch values.

A moving-point optimization carried out at 9° collective pitch yielded the following optimal aeroelastic couplings:

$$K_{P\beta} = 0.6288 \qquad K_{P\zeta} = -1.0$$
$$R_{\beta} = 1.0 \qquad R_{\zeta} = 0.0 \tag{17}$$

Figure 21 shows that these couplings result in very large stability margins at high collective pitch values, but the damping decreases with decreasing collective. Eventually, the regressing lag mode becomes unstable at $\theta_o < 5°$, and for $\theta_o < 2°$, the damping in the regressing lag mode falls to values lower than the baseline configuration (no aeroelastic couplings).

It should be noted that the optimal aeroelastic couplings at 0° collective (Eq. 16) are fundamentally different from the optimal couplings for moderate or high collective pitch (Eqs. 15 and 17).

Multi-Point Optimization at 0° and 9°

In an attempt to stabilize ground resonance over a wide range of variation in thrust conditions, the previously described moving-point optimization procedure is simultaneously implemented at two different collective pitch settings - 0° and 9°. The objective function to be minimized is:

$$F(D_j) = W^{0°}(\sigma_{min} - \overline{\sigma}_{min})^2_{0°} + W^{9°}(\sigma_{min} - \overline{\sigma}_{min})^2_{9°} \tag{18}$$

subject to constraints on design variables, Eq. 9. The optimization procedure yielded the following results:

$$K_{P\beta} = 0.814 \qquad K_{P\zeta} = -0.221$$
$$R_{\beta} = 1.0 \qquad R_{\zeta} = 0.0 \tag{19}$$

Figure 21 indicates that while simultaneous optimization at 0° and 9° is unable to completely stabilize the regressing lag mode, the level of instability is restricted to a fairly modest value over a broad range of variation in collective pitch, and the destabilizing trend with increasing collective pitch seen in the baseline configuration is alleviated. It is also seen that there is no collective pitch at which the regressing

lag mode damping is lower than that of the baseline. Up to a collective pitch of 5° the minimum damping in the regressing lag mode remains fairly uniform, and then starts to slowly increase.

Attempts to further increase the minimum damping at low to moderate values of collective pitch by varying the weights $W_{0}o$ and $W_{9}o$ were unsuccessful. Even though it appears in Figure 21 that it should be possible to trade stability margin at high thrust conditions for increased damping at lower collective pitch, the aeroelastic coupling requirements are such that large decreases in stability at high collective resulted in only very small increases in stability at low collective.

Similarly, no significant improvement in minimum lag damping was obtained for optimization at a different set of collective pitch values. For example, when multi-point optimization was carried out simultaneously at 0° and 5° the results were similar to those obtained by optimizing at 0° and 9°.

Two-Stage Optimization

The final objective function formulation addresses some of the shortcomings of the previous formulations described above. Rather than attempting to achieve some prescribed level of regressing lag mode damping, $\overline{\sigma}$, the objective function is formulated to increase lag mode damping as much as possible, by maximizing the decay rate of the lag mode. This is a more general formulation, and the optimized results obtained are not affected by arbitrarily chosen levels of prescribed damping. Furthermore, instead of addressing conflicting stability requirements at high and low collective pitch settings by conducting multi-point optimization, the objective function now allows the design point to move to different values of collective pitch, as well as rotational speed. The objective function selected in the present study is:

$$F(D_j) = \sigma_{min} \tag{20}$$

where D_j represents the vector of design variables, and σ_{min} represents the regressing lag mode decay rate at the rotational speed (Ω) and collective pitch (θ) corresponding to minimum damping. As the values assigned to the various design variables change during the optimization process, the point of minimum damping moves to a different rotational speed and collective pitch setting. So for each iteration in the optimization procedure, the rotational speed and collective pitch corresponding to minimum damping is determined and the optimization process is continued at this new point (Ω_{min}, θ_{min}).

Initially, σ_{min} was determined by conducting a sweep of rotor speed and collective pitch settings, and for each iteration, selecting the (Ω_{min}, θ_{min}) point of lowest damping. It was observed, however, that the optimization procedure was very sensitive to discretization errors in locating the point of minimum damping. The gradients of the design variables at a rotor speed just above the point of minimum damping were quite different, for example, from the gradients at the point of minimum damping. Figure 22 illustrates this phenomenon. If stability is examined at discrete values of Ω (a finite number of points), consider the following scenario: stability is examined at 30 RPM intervals 730, 760, 790 RPM, etc. Thus the point of minimum damping for the case $K_{P\zeta} = -0.4$ would be determined as 760 RPM (Point A). At this value of Ω, negative $K_{P\zeta}$ would be stabilizing. However, the actual point of minimum damping is 750 RPM (Point B). At this value of Ω, negative $K_{P\zeta}$ is destabilizing, whereas at 760 RPM negative $K_{P\zeta}$ has a stabilizing influence. Therefore the sensitivity gradients determined at 760 RPM would be of opposite sign, compared to those determined at 750 RPM. Thus the discretization errors introduced cause significant difficulties in convergence and compromise the robustness of the optimization process (making it numerically inefficient). In order for the optimization procedure to converge, an inordinately fine grid of rotor speed and collective pitch had to be swept. The computation time required to perform such an optimization was extremely high.

To more efficiently determine the point of minimum damping, an inner loop was introduced in the optimization procedure with the goal of finding, precisely, the point (Ω_{min}, θ_{min}) corresponding to minimum lag mode damping for a *set of prescribed values for the design variables* D_j. In the inner loop, the following function was minimized:

$$F(\overline{D}_k) = -\sigma_{lag} \tag{21}$$

where σ_{lag} represents the decay rate of the regressing lag mode for a fixed design ($K_{P\beta}$, $K_{P\zeta}$, R_β, R_ζ, ΔK_β, ΔK_ζ). For each iteration of the optimization process, this inner loop first determines values of the operational parameters $\overline{D}_k(\Omega, \theta)$ which define the point of minimum lag damping (Ω_{min}, θ_{min}). Minimization of the objective function in Eq. 20 is continued at this point. Sensitivity gradients of the design variables, $\frac{\partial \sigma_{min}}{\partial D_j}$, are calculated, and new values for the design variables are determined. This process is repeated until optimality is achieved. Figure 23 provides an outline of this algorithm.

This two-stage optimization procedure is clearly superior to a brute force approach for determining σ_{min}. There are no robustness issues resulting from discretization errors. It is a numerically efficient approach

that converges quickly. The two-stage optimization approach reduces computation time tremendously, requiring far fewer calls to the eigenvalue solver subroutine, approximately 10 calls per iteration, compared to 1000 for the old technique of conducting a sweep in θ and Ω.

The primary optimization design variables are subject to the following constraints:

$$\begin{aligned} -1.0 \le K_{P\beta} \le 1.0 \qquad & -1.0 \le K_{P\zeta} \le 1.0 \\ 0.0 \le R_{\beta} \le 1.0 \qquad & 0.0 \le R_{\zeta} \le 1.0 \\ -0.25 \le \Delta K_{\beta} \le 0.25 \qquad & -0.25 \le \Delta K_{\zeta} \le 0.25 \end{aligned} \tag{22}$$

The range of allowable values for ΔK_{β} and ΔK_{ζ} represent a permitted change in blade flexural stiffness of ±25%. This range of stiffness values is regarded as sufficient to have an influence on aeromechanical stability characteristics, while preventing unrealistically large dynamic stresses in the flexure.

Further constraints were enforced to keep the rotor's rotating flap and lag frequencies within reasonable bounds. These constraints were formulated as follows:

$$\begin{aligned} 1.07 \cdot \Omega_0 \le \omega_{\beta} \le 1.15 \cdot \Omega_0 \\ 0.6 \cdot \Omega_0 \le \omega_{\zeta} \le 0.8 \cdot \Omega_0 \end{aligned} \tag{23}$$

where Ω_0 is the rotor's nominal operating speed, and ω_{β} and ω_{ζ} are, respectively, the rotor flap and lag rotating modal frequencies (represented in this analysis by the modal frequencies of the collective flap and lag modes obtained from the eigen-analysis).

Optimization Results

The optimization process was applied to four different test cases: *(i)* aeroelastic couplings alone considered as design variables, and no frequency constraints, *(ii)* blade flap and lag stiffness parameters introduced as additional design variables, no frequency constraints, *(iii)* aeroelastic couplings alone, with frequency constraints, and *(iv)* aeroelastic couplings plus blade stiffness parameters, with frequency constraints.

Aeroelastic Couplings Only: No Frequency Constraints

When using only the aeroelastic couplings as design variables, and placing no constraints on the rotor flap and lag frequencies, the optimization procedure yields the following results:

$$K_{P\beta} = 0.7966 \qquad K_{P\zeta} = -0.2539$$
$$R_{\beta} = 1.0 \qquad R_{\zeta} = 0.0 \tag{24}$$

Figure 24 shows the stability characteristics (minimum decay rate at roll resonance) of this configuration as compared to the baseline, across the collective pitch range. At the flat pitch condition, the two configurations share roughly the same level of instability. As collective pitch increases, however, the baseline rotor rapidly becomes less stable. When the aeroelastic coupling parameters given in Eq. 24 are applied, this destabilizing trend is reversed, and the rotor becomes more stable as collective pitch is increased. However, the large amount of pitch-flap coupling in this configuration causes a large increase in the rotor's flap frequency, to 1.32 /rev, which may be undesirable from other perspectives such as handling qualities. The lag frequency of 0.685 /rev of the baseline rotor was unchanged.

Aeroelastic Couplings plus Flap, Lag Stiffness: No Frequency Constraints

When the flap and lag stiffness parameters are included as design variables in the optimization procedure, the following results are obtained:

$$K_{P\beta} = 0.7317 \qquad K_{P\zeta} = -0.2328$$
$$R_{\beta} = 1.0 \qquad R_{\zeta} = 0.0 \tag{25}$$
$$\Delta K_{\beta} = 0.25 \qquad \Delta K_{\zeta} = 0.25$$

The stability characteristics for the new configuration as a function of collective pitch are included on Figure 24. The stability trend is the same as for the case with optimized couplings alone, but the inclusion of stiffness parameters in the optimization allows for further reduction of the instability. As before, the configuration defined by Eq. 25 produces an undesirably high flap frequency of 1.31 /rev, while the lag frequency is now increased to 0.739 /rev.

Note that in Eq. 25 the values for ΔK_{β} and ΔK_{ζ} have reached the upper bounds that were imposed on these variables in Eq. 22. This is consistent with the observations made from the parametric study that

increasing values of blade flap and lag stiffness have a stabilizing effect on ground resonance. Meanwhile, the values obtained for the aeroelastic coupling parameters are similar to those obtained in Eq. 24, when the aeroelastic coupling parameters alone were optimized.

Aeroelastic Couplings Only: Frequency Constraints Applied

The results presented thus far showed that the incorporation of aeroelastic couplings, along with modifications to rotor stiffness properties, can have a significant stabilizing effect on ground resonance instability. However, along with this stabilizing influence came a large increase in the rotor's rotating flap frequency. In order to address this undesirable effect, the constraints given in Eq. 23 were added to the analysis. For the case where the design variables consist of only the aeroelastic couplings, adding these constraints yielded the following optimized results:

$$K_{P\beta} = 0.3376 \qquad K_{P\zeta} = -0.2315$$
$$R_{\beta} = 1.0 \qquad R_{\zeta} = 0.0 \tag{26}$$

Figure 25 shows the stability characteristics for a configuration using these coupling parameters, compared to the baseline rotor. The present configuration behaves much like the previous cases where no frequency constraint was applied, but it is not able to stabilize the system to the same degree (compare with Figure 24). Comparing the results in Eq. 26 to those in Eq. 24 shows that the introduction of frequency constraints on the rotor reduces the amount of pitch-flap coupling that is permitted. With the coupling parameters given in Eq. 26, the rotor is operating with a rotating flap frequency of 1.15 /rev (as calculated from the solution of the eigenvalue problem) which is the upper limit imposed on the optimization process by Eq. 23. So the constraint on flap frequency prevents $K_{P\beta}$ from reaching the value it would normally attain if the constraint was absent or relaxed. This reduced value of $K_{P\beta}$ is responsible for the slight reduction in stabilizing effect when compared to the results with no frequency constraints. The rotating lag frequency was calculated at 0.685 /rev, so the constraints on lag frequency in Eq.23 were not active.

Aeroelastic Couplings plus Flap, Lag Stiffness: Frequency Constraints Applied

The optimization procedure was repeated, incorporating the frequency constraints, as well as the flap and lag stiffness design variables. The process yielded the following values for the design variables:

$$K_{P\beta} = 0.3192 \qquad K_{P\zeta} = -0.2157$$

$$R_{\beta} = 1.0 \qquad R_{\zeta} = 0.0 \qquad (27)$$

$$\Delta K_{\beta} = 0.25 \qquad \Delta K_{\zeta} = 0.25$$

Figure 25 shows that this configuration closely follows the same stability trends as the configuration described by Eq. 26, but exhibits a decrease in the level of instability. For this optimized design (Eq. 27), ΔK_{β} and ΔK_{ζ} again reached their upper bounds (as was the case without frequency constraints, Eq. 25). The aeroelastic coupling parameters were similar to those obtained without considering stiffness as design variables (compare with Eq. 26). This same behavior was noted for the cases with no frequency constraints (compare Eq. 24 and Eq. 25). For both cases with frequency constraints, limiting the rotating flap frequency to a predetermined value causes $K_{P\beta}$ to be reduced in magnitude when compared to the values obtained when no frequency constraints were enforced. It is also interesting to note that the incorporation of blade stiffness parameters into the optimization returns the level of damping to roughly that achieved by aeroelastic couplings alone with no frequency constraints. However, this level of damping is now achieved without excessively large values of rotating flap frequency. The rotating lag frequency was again inside the bounds set by the constraints in Eq. 23.

Sequential vs. Concurrent Optimization

The coupling and stiffness parameters presented in Eqs. 25 and 27 were obtained through a *concurrent* optimization process, where both aeroelastic couplings and blade stiffness parameters are simultaneously optimized to improve helicopter aeromechanical stability. For comparison purposes, a series of *sequential* optimizations was performed, where the aeroelastic couplings and the blade stiffness parameters were considered as two independent groups of design variables. Optimizations were conducted holding one group at its baseline values while optimizing the other group. These optimized values were then held while the first group was optimized.

Sequential Optimization: No Frequency Constraints

The sequential optimization approach was employed with no constraints applied to blade flap or lag frequencies. Optimizing the blade stiffness parameters, then the aeroelastic couplings yielded the following results:

$$K_{P\beta} = 0.8067 \qquad K_{P\zeta} = -0.2385$$

$$R_{\beta} = 1.0 \qquad R_{\zeta} = 0.0 \tag{28}$$

$$\Delta K_{\beta} = 0.25 \qquad \Delta K_{\zeta} = -0.1058$$

Optimizing the aeroelastic couplings first, then the blade stiffness parameters produced these values:

$$K_{P\beta} = 0.7966 \qquad K_{P\zeta} = -0.2539$$

$$R_{\beta} = 1.0 \qquad R_{\zeta} = 0.0 \tag{29}$$

$$\Delta K_{\beta} = 0.25 \qquad \Delta K_{\zeta} = 0.25$$

Figure 26 shows the stability characteristics of these two configurations, along with the concurrently optimized case (Eq. 25). The optimized designs of Eq. 25 and Eq. 29 are similar, and Figure 26 shows that they perform almost identically. The concurrently optimized results outperform the couplings-first, stiffness-second sequentially optimized results numerically by only the slimmest of margins (of no practical relevance). These results demonstrate the fact that the optimal configuration is not overly sensitive to small changes in the design variables. Even for a somewhat off-design configuration, most of the stabilizing effect remains intact.

Figure 26 also shows that the sequentially optimized case where the stiffness parameters are optimized before the aeroelastic couplings has noticeably poorer performance. Examining the parameters in Eq. 28 reveals a difference in the blade lag stiffness parameter, ΔK_{ζ}. For this sequentially optimized case, the blade stiffness parameters were optimized first. Without the influence of aeroelastic couplings, the point of minimum damping occurred at a high value of collective pitch. Figure 16 showed that for high values of collective pitch, increased lag stiffness was destabilizing. Thus for an optimization performed on stiffness parameters alone, a negative ΔK_{ζ} (decreasing lag stiffness) was found to be beneficial. However, the aeroelastic couplings introduced in the second step of this optimization procedure shifted the point of minimum damping to a much lower value of collective pitch, where the decreased lag stiffness was now in fact detrimental to stability.

Sequential Optimization: Frequency Constraints Applied

The sequential optimization approach was employed while enforcing the constraints on blade flap or lag frequencies (Eq. 23). Optimizing the blade stiffness parameters, then the aeroelastic couplings yielded the following results:

$$\begin{aligned} K_{P\beta} &= 0.3190 & K_{P\zeta} &= -0.2170 \\ R_{\beta} &= 1.0 & R_{\zeta} &= 0.0 \\ \Delta K_{\beta} &= 0.25 & \Delta K_{\zeta} &= -0.1058 \end{aligned} \tag{30}$$

Optimizing the aeroelastic couplings first, then the blade stiffness parameters produced these values:

$$\begin{aligned} K_{P\beta} &= 0.3376 & K_{P\zeta} &= -0.2315 \\ R_{\beta} &= 1.0 & R_{\zeta} &= 0.0 \\ \Delta K_{\beta} &= 0.002803 & \Delta K_{\zeta} &= 0.25 \end{aligned} \tag{31}$$

Figure 27 shows the stability characteristics of these two configurations, along with the concurrently optimized case (Eq. 27). We notice again that the stiffness-first, couplings-second sequentially optimized case (Eq. 30) does not perform as well as the other cases, because of the negative value of ΔK_{ζ}. There is also now a more noticeable difference between the couplings-first, stiffness-second sequential case (Eq. 31) and the concurrently optimized case. In Eq. 31, ΔK_{β} is held to a very small value, representing almost no change in flap stiffness from the baseline value. Also note that $K_{P\beta}$ is slightly higher than in the case of concurrent optimization (Eq. 27). These two parameters both have a significant effect on the rotor rotating flap frequency. Increasing values of either parameter increases the flap frequency. In the case of the couplings-first sequential optimization, $K_{P\beta}$ was optimized while ΔK_{β} was held at zero. This allowed $K_{P\beta}$ to reach a higher value, when compared to the concurrent optimization results. Since the upper bound on flap frequency had been reached already by the aeroelastic couplings, ΔK_{β} could not be increased during the second step of the sequential optimization process. It is this difference in flap stiffness parameters between Eq. 27 and Eq. 31 that explain the gap in performance between the couplings-first sequential configuration, and the concurrently optimized configuration.

Influence of Relaxed Frequency Constraints

The bounds on frequency constraints given in Eq. 23 were selected to represent typical rotating flap and lag frequencies. When these constraints are applied to the optimization process, only the upper constraint on flap frequency becomes active. Figure 28 shows how the level of minimum damping changes as the upper bound on the flap frequency is increased from a value of 1.12 /rev to 1.35 /rev. The level of damping increases rapidly at first, and then begins to taper off. By the time the constraint reaches 1.32 /rev, further increases have no effect, because the system has reached the optimum point obtained when frequency constraints were not enforced. As the constraint is increased beyond this value, it is no longer active.

Suitability of Gradient – Based Optimization

The optimization results presented here have been obtained via a gradient-based optimization scheme. For any optimization problem, there exists the potential for multiple optimal points within the design space (the set of all possible combinations of design variables). If multiple optimal points exist within the design space, the solution obtained by a gradient-based optimizer becomes dependent upon initial guess. The optimizer will follow the gradients until an optimal point is encountered, and stop there. Depending on the initial starting point chosen for optimization, different optimal points may be reached, yielding different solutions to the problem. Furthermore, a gradient-based optimization is unable to distinguish between an optimal point that may simply be a local minimum in the design space, and the global minimum, so there is no guarantee that a given solution represents the best solution to the optimization problem.

Non-gradient based optimization techniques, such as genetic algorithms (GA), or simulated annealing, are not susceptible to these difficulties, and are thus able to obtain a globally optimal solution even in the presence of multiple optimal points. Non-gradient based optimizations, however, are much more computationally expensive than gradient-based optimizations. Gradient-based optimization is therefore the preferred approach, provided the design space for the optimization problem in question does not contain multiple optimal points.

In order to determine the suitability of gradient-based optimization for the present application, it is necessary to examine the design space, to ensure that there are not multiple optimal points. The fact that the current optimization procedure converges to the same optimal solution regardless of the initial guess chosen for the design variables is a good indication that there is only one optimal point in the design

space. However, a more thorough investigation of the design space is required to support this observation.

Figure 29 is an illustration of the sensitivity of the system to each individual design variable, for the baseline configuration (all other design variables set to zero). The slope of each curve is a measure of the particular design variable's gradient (value of sensitivity derivative), with a positive slope indicating stabilizing effect for increasingly positive values of the design variable. A zero slope indicates a potentially optimal point for a given design variable. It can be seen in Figure 29 that at the baseline condition (zero on the x-axis), positive pitch-flap and negative pitch-lag couplings have the strongest beneficial effect on stability. Furthermore, there is no indication of multiple optimal points within the design space for any of the design variables.

Figure 30 repeats this information for the concurrently optimized configuration including stiffness parameters and frequency constraints (Eq. 27). The actual optimized value of each design variable is indicated on the figure. It can be seen that design variables R_β, R_ζ, ΔK_β, and ΔK_ζ all reach the bounds placed on them by Eq. 22. $K_{P\zeta}$ achieves a value where it's gradient is zero, indicating an optimal value has been reached, unaffected by any constraints. $K_{P\beta}$, however, has not reached the bounds placed on it by Eq. 22, nor is its gradient zero. It is being held to this value by the frequency constraints imposed by Eq. 23. If these frequency constraints were relaxed, $K_{P\beta}$ would attain a value of approximately 0.75, where there is a plateau in its sensitivity curve. Indeed, Eq. 24 and Eq. 25 show that this in fact the case. Figure 30 also provides no indication of multiple optimal points for any design variable.

Due to the number of design variables involved in the present analysis, it is difficult to visualize the design space as a whole. It is possible to examine "slices" of the design space. Figure 31 is such a "slice" of the design space, showing the variation of lag mode decay rate with $K_{P\beta}$ and $K_{P\zeta}$, the two most powerful design variables, at a collective pitch of 5°. The contour lines in Figure 31 represent lines of constant decay rate. Lag mode stability is seen to steadily increase as one moves towards the lower right corner of Figure 31. Nowhere are there closed contours at separate locations on the plot, which would indicate multiple optimal points within this "slice" of the design space.

Plots similar to Figure 31 were generated for different values of collective pitch, and all exhibited similar trends. Thus it is felt that there are no multiple optimal points in the design space, and a gradient-based optimization technique is appropriate for this investigation.

Variations in Body Frequency

The present study has investigated the influence of rotor parameters (aeroelastic couplings, rotor stiffness) on aeromechanical stability. Body properties, such as frequency and damping, also have an important effect on helicopter aeromechanical stability. The helicopter designer can influence these properties by modifying certain design parameters, such as landing gear stiffness. They are also affected in operation by variations in configuration, such as changes in payload or fuel. The present optimized configuration (Eq. 27) was obtained using the nominal body properties presented in Table 1. It is essential that the optimized configuration be robust and maintain its stabilizing influence on ground resonance for variations in body properties which occur in operation.

The effectiveness of the optimized configuration was examined at off-design conditions by allowing body roll inertia to vary by ±20%. Figure 32 shows variation in minimum damping versus roll inertia for the optimized configuration (from Eq. 27) as well as the baseline model. In both cases, there exists a destabilizing trend as roll inertia is decreased (roll frequency increased). However, the optimized configuration maintains its stability increase over the baseline, over the entire range of roll inertia variation. Since body inertia may change with variations in fuel or payload on a helicopter, the present results indicate that the minimum inertia configuration should be treated as the critical design point for alleviating ground resonance. If adequate stability margins are achieved for minimum inertia, stability is assured as inertia increases.

Figure 33 shows the influence of body roll stiffness on ground resonance. It can be seen that increased roll stiffness aggravates the instability, while reduced roll stiffness alleviates the instability. This is consistent with observations reported in [18], where vertically soft landing gear configurations were found to be beneficial for reducing ground resonance instabilities. However, increased roll stiffness does move the instability to higher rotational speeds. These observations suggest that there are two approaches to selecting roll stiffness values to avoid resonance conditions. First, roll stiffness (due to landing gear) can be increased as much as possible, to move the instability to a rotor speed above the operational speed. However, operational conditions can reduce roll frequency, through increased payload (increased roll inertia) or operation from soft, unimproved surfaces. For this approach to be successfully employed, the roll stiffness must be increased to the point that even for the case of maximum payload (max roll inertia), the resonance speed still remains comfortably above the operating speed. However, it should be noted that very high landing gear stiffness may result in high impact loads during landing.

The second approach to improving ground resonance stability by changing the landing gear roll stiffness is to soften the landing gear as much as is practical, to produce a much milder instability. The relatively mild instability can then be stabilized through the use of appropriate rotor aeroelastic coupling and stiffness parameters. To ensure adequate stability margins at all operating conditions, stability must be achieved for the case of zero payload, corresponding to the case of minimum possible roll inertia. If stability is achieved at that point, any reduction in roll frequency due to an increase in roll inertia (from increased payload), will only increase the level of stability and resonance will occur at even lower rotational speeds. Figure 34 shows the aeromechanical stability characteristics, using optimized aeroelastic couplings (Eq. 27) from the present investigation, along with a reduced landing gear roll stiffness. It is seen that the system has become marginally stable, without the use of an auxiliary lag damper.

A reduction in roll stiffness on the order of 40% may not be generally regarded as feasible for many practical applications, due to the resulting large static deflection of the landing gear (in the vertical direction). It is possible, however, to design a landing gear that retains a larger amount of vertical stiffness to support the weight of the helicopter, while at the same time allowing enough flexibility in roll to help alleviate ground resonance [19]. Furthermore, aeromechanical stability may perhaps best be attained through a combination of several parameters. By incorporating concurrently optimized couplings and rotor stiffness parameters to yield a mild level of instability over a broad range of conditions, adequate levels of lag mode damping may be achieved with small increases in landing gear damping, and/or a modest reduction in body roll stiffness. The small contribution from each parameter, when combined, may be able to provide the required aeromechanical stability margin. Such an approach offers the most promise for elimination of auxiliary lag dampers on rotor blades.

Effect of Optimized Results on Air Resonance Stability

Each of the optimized configurations presented in this study was examined in hover to ensure adequate stability margins to avoid air resonance instabilities. For the hover condition, each case was trimmed to a constant thrust, with a nominal C_T/σ of 0.07, and body support stiffness and damping were set to zero. Figure 35 shows the air resonance stability characteristics in hover for the baseline configuration as well as the optimized configuration (Eq. 27). The optimized configuration shows greatly increased stability margins near the rotor nominal operating speed, compared to the baseline model.

Figure 36 shows lag mode stability characteristics for the baseline and optimized configurations in forward flight, at an advance ratio of 0.3. The rotor was trimmed to a constant thrust (nominal C_T/σ of 0.07), zero first harmonic flapping, and 3° of forward shaft tilt was specified. Again, as in the case of hovering flight, the optimized configuration exhibits increased air resonance stability margins near the nominal rotor speed.

Figure 37 compares the stability of the baseline configuration with that of the optimized design given in Eq. 27, for increasing advance ratio. It can be seen that the baseline configuration exhibits increasing levels of stability as advance ratio increases. The optimized configuration follows a similar trend, and provides increased stability over the baseline at all values of advance ratio.

Figure 38 illustrates the influence of variations in roll inertia on air resonance stability in hover and at an advance ratio of 0.3 for both the baseline and optimized design. The stability trends in each case remain similar to what was observed for the ground contact condition – a reduction in body roll inertia yields a decrease in stability. Again, this indicates that if the optimized design has adequate stability margins at minimum inertia, increases in body inertia will only increase the stability margin.

Summary and Concluding Remarks

Aeroelastic couplings have been shown to have a significant influence on helicopter aeromechanical instability. Formal optimization techniques are able to determine the optimal combination of couplings to maximize regressing lag damping. The inclusion of rotor stiffness properties as concurrent design variables adds power and flexibility to this optimization process, allowing significant stability augmentation, without large changes in rotor flap and lag frequencies. By utilizing optimized aeroelastic couplings and rotor stiffness properties, along with careful selection of body stiffness and damping properties, a damperless yet aeromechanically stable design may be possible.

1) The two-stage optimization algorithm developed in the present study is robust and numerically efficient, converging quickly to the optimal solution.

2) Most of the stabilizing effect from aeroelastic coupling parameters is maintained when placing constraints on the rotor rotational flap and lag frequencies. By introducing the rotor flap stiffness as a design parameter, the stability margin lost by enforcing frequency constraints can be largely regained.

3) Concurrently optimizing both aeroelastic couplings and blade stiffness parameters provides the greatest effectiveness in increasing aeromechanical stability, while at the same time satisfying constraints on rotor flap and lag frequencies. If a sequential optimization approach is used, optimizing aeroelastic couplings before the blade stiffness parameters provides a greater increase in stability than the reverse order of optimizing first stiffness then coupling parameters.

4) Relaxing the flap frequency constraints results in improvements in stability. This is a result of the larger values of pitch-flap coupling allowed by the increased upper bound on flap frequency. As the constraints are further relaxed, the beneficial effect decreases.

5) There is no indication of multiple optimal points within the design space for this problem. This indicates that gradient-based optimization techniques are suitable for optimizing aeroelastic couplings and rotor stiffness properties.

6) The optimized configurations examined here share with the baseline model a destabilizing trend with decreasing roll inertia. The minimum-inertia condition is a critical design point: if adequate stability margins are achieved at minimum inertia, any increase in inertia will increase the stability margin.

7) Reducing the roll stiffness of the landing gear can have a beneficial effect by reducing the magnitude of the ground resonance instability. When optimized aeroelastic couplings, rotor stiffness parameters, landing gear damping, and reduced roll stiffness are used in combination, there is a potential to stabilize the rotor across the entire operating range, eliminating the need for auxiliary lag dampers.

8) Air resonance stability margins are significantly improved in all optimized configurations examined, both in hover and for forward flight.

Publications

"Optimized Aeroelastic Couplings for Alleviation of Helicopter Ground Resonance", Proceedings of 37th AIAA/ASME/ASCE/AHS/ASC Structures, Structural Dynamics, and Materials Conference, Orlando, FL, April 21-24, 1997.

"Optimized Aeroelastic Couplings for Alleviation of Helicopter Ground Resonance", AIAA Journal of Aircraft, Vol. 35, No. 4, July-August, 1998, pp. 582-589.

"Concurrent Optimization of Aeroelastic Couplings and Rotor Stiffness for the Alleviation of Helicopter Aeromechanical Instability", Proceedings of the 55th annual AHS Forum, Montreal, Canada, May 25-27, 1999; also presented at 8th International Workshop on Dynamics and Aeroelastic Modeling of Rotorcraft, University Park, PA, Oct. 18-20, 1999.

"Individual Blade Control for Alleviation of Helicopter Ground Resonance", Proceedings of the 38th AIAA/ASME/ASCE/AHS/ASC Structures, Structural Dynamics, and Materials Conference, Long Beach, CA, April 20-23, 1998.

"Use of Aeroelastic Couplings for Alleviation of Helicopter Aeromechanical Instability", AIAA Journal of Aircraft, accepted.

Participating Personnel

Dr. Farhan Gandhi, Principal Investigator

Eric Hathaway, Graduate Research Assistant – earned MS in Aerospace Engineering from the Pennsylvania State University

Phuriwat Anusonti-Inthra, Graduate Research Assistant – earned MS in Aerospace Engineering from the Pennsylvania State University

Bibliography

[1] Chopra, I., "Perspectives in Aeromechanical Stability of Helicopter Rotors," *Vertica*, Vol. 14, No. 4, 1990.

[2] Ormiston, R. A., "The Challenge of the Damperless Rotor," Proceedings of the 22nd European Rotorcraft Forum, Brighton, England, September 17-19, 1996.

[3] Gandhi, F., "Concepts for Damperless Aeromechanically Stable Rotors," Proceedings of the Royal Aeronautical Society Innovation in Rotorcraft Technology Conference, London, UK, June 24-25, 1997.

[4] Ormiston, Robert A., "Techniques for Improving the Stability of Soft Inplane Hingeless Rotors," NASA TN X-62390, October 1974.

[5] Bousman, W. G., Sharpe, D. L., and Ormiston, R. A., "An Experimental Study of Techniques for Increasing the Lead-Lag Damping of Soft Inplane Hingeless Rotors," Proceedings of the 32nd Annual National V/STOL Forum of the American Helicopter Society, Washington D.C., May 1976.

[6] Bousman, William G., "The Effects of Structural Flap-Lag and Pitch-Lag Coupling on Soft Inplane Hingeless Rotor Stability in Hover," NASA Technical Paper 3002, May 1990.

[7] Ormiston, Robert A., "Aeromechanical Stability of Soft Inplane Hingeless Rotor Helicopters," Paper No. 25, Third European Rotorcraft and Powered Lift Aircraft Forum, Aix-en-Provence, France, September 7-9, 1977.

[8] Bousman, William G., "An Experimental Investigation of the Effects of Aeroelastic Couplings on Aeromechanical Stability of a Hingeless Rotor Helicopter," *Journal of the American Helicopter Society*, Vol. 26, No. 1, January 1981, pp. 46-54.

[9] Ormiston, Robert A., "Investigations of Hingeless Rotor Stability," *Vertica*, Vol. 7, No. 2, 1983, pp. 143-181.

[10] King, S. P., "The Effect of Pitch-Flap and Pitch-Lag Coupling on Air Resonance," Westland Helicopters Limited, Yeovil, Dynamics Department Report, No. GEN/DYN/RES/005R, July 1971.

[11] Nagabhushanam, J., and Gaonkar, G. H., "Rotorcraft Air Resonance in Forward Flight with Various Dynamic Inflow Models and Aeroelastic Couplings," Paper No. 52, Ninth European Rotorcraft Forum, Stresa, Italy, September 13-15, 1983.

[12] Zotto, M. D., and Loewy, R. G., "Influence of Pitch-Lag Coupling on Damping Requirements to Stabilize Ground/Air Resonance," *Journal of the American Helicopter Society*, Vol. 37, No. 4, October 1992, pp. 68-71.

[13] Milgram, J. H., and Chopra, I., "Air Resonance of Hingeless Rotor Helicopters in Trimmed Forward Flight," *Journal of the American Helicopter Society*, Vol. 39, No. 4, October 1994, pp. 46-58.

[14] Venkatesan, C., "Influence of Aeroelastic Couplings on Coupled Rotor/Body Dynamics," Presented at the Sixth International Workshop on Dynamics and Aeroelastic Stability Modeling of Rotorcraft Systems, Los Angeles, California, Nov. 8-10, 1995.

[15] Gandhi, F. and Hathaway, E., "Optimized Aeroelastic Couplings for Alleviation of Helicopter Ground Resonance," *Journal of Aircraft*, Vol. 35, No. 4, July-Aug. 1998, pp. 582-589.

[16] Ormiston, R. A., and Hodges, D. H., "Linear Flap-Lag Dynamics of Hingeless Helicopter Rotor Blades in Hover," *Journal of the American Helicopter Society*, Vol. 17, No. 2, 1972, pp. 2-15.

[17] Takahashi, M. D., and Friedmann, P. P., "Active Control of Helicopter Air Resonance in Hover and Forward Flight," AIAA Paper No. 88-2407, Proceedings of the 29th AIAA/ASME/ASCE/AHS Structures, Structural Dynamics, and Materials Conference, Williamsburg, Virginia, April 18-20, 1988, pp. 1521-1532.

[18] Lytwyn, R. T., Miao, W., and Woitsch, W., "Airborne and Ground Resonance of Hingeless Rotors," *Journal of the American Helicopter Society*, Vol. 16, No. 2, April 1971, pp. 2-9.

[19] Cardin, V., "Practical Examples of New Technologies in Dynamics as Applied to Eurocopter Products," Proceedings of the 56th Annual Forum of the American Helicopter Society, Virginia Beach, Virginia, May 2-4, 2000.

Tables and Figures

Table 1: Rotor - Fuselage Properties

Rotor Properties	
Number of blades	3
Radius, cm	81.1
Chord, cm	4.19
Hinge offset, cm	8.51
Lock number	7.37
Blade profile	NACA 23012
Profile drag coefficient	0.0079
Flap inertia, g-m^2	17.3
Polar inertia, g-m^2	85.5
Non-rotating flap freq., Hz	3.13
Non-rotating lag freq., Hz	6.70
Lag damping, %	0.52

Body Properties		
	Roll	Pitch
Inertia, g-m^2	183	633
Frequency, Hz	4.0	2.0
Damping, %	0.929	3.20

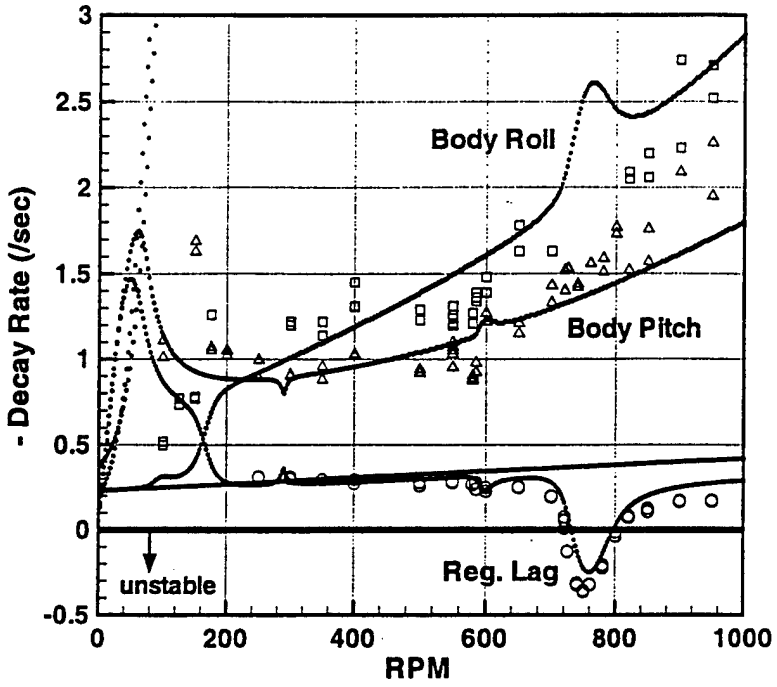

Fig 1: Modal damping vs. rotational speed at 0° collective

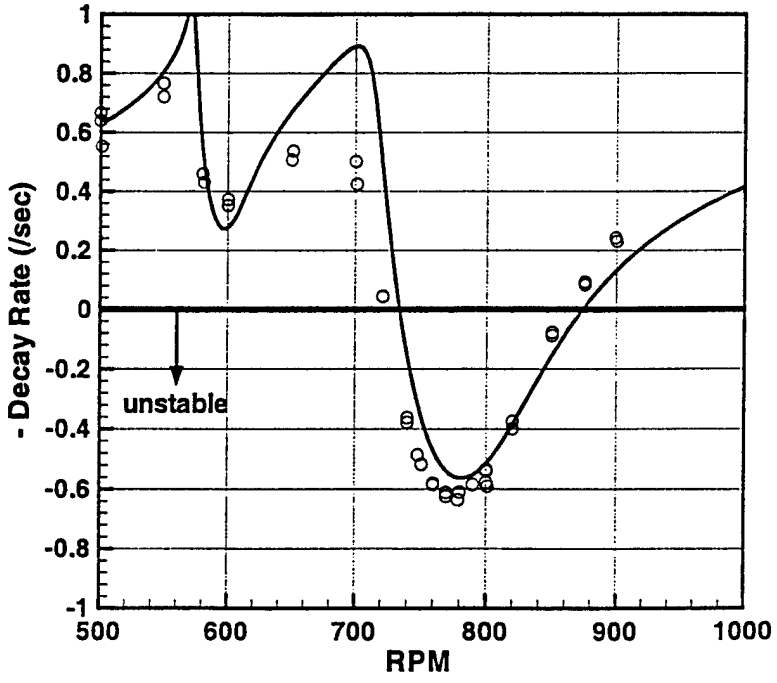

Fig 2: Variation of regressing lag damping vs. rotational speed at 9° collective

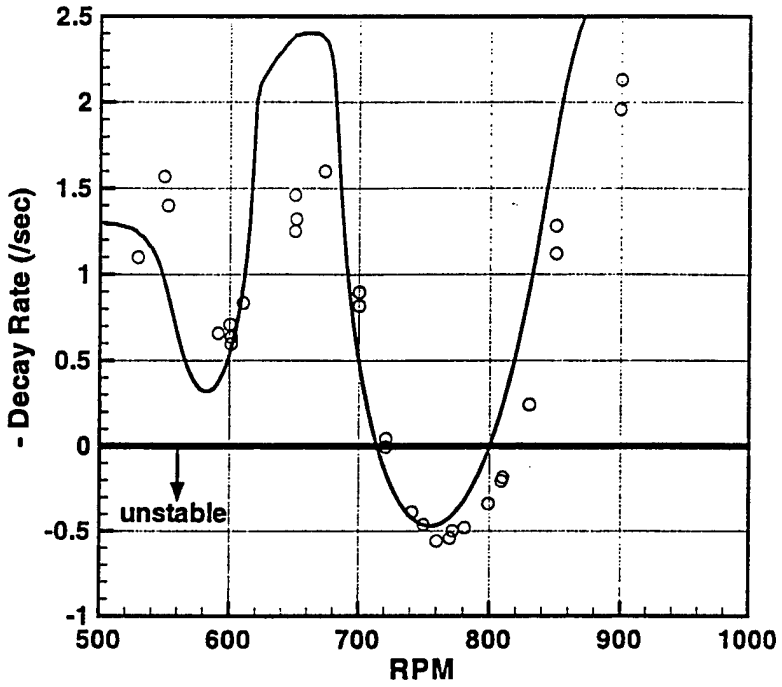

Fig 3: Variation of regressing lag damping vs. rotational speed at 9° collective ($K_{P\zeta}$ = -0.4)

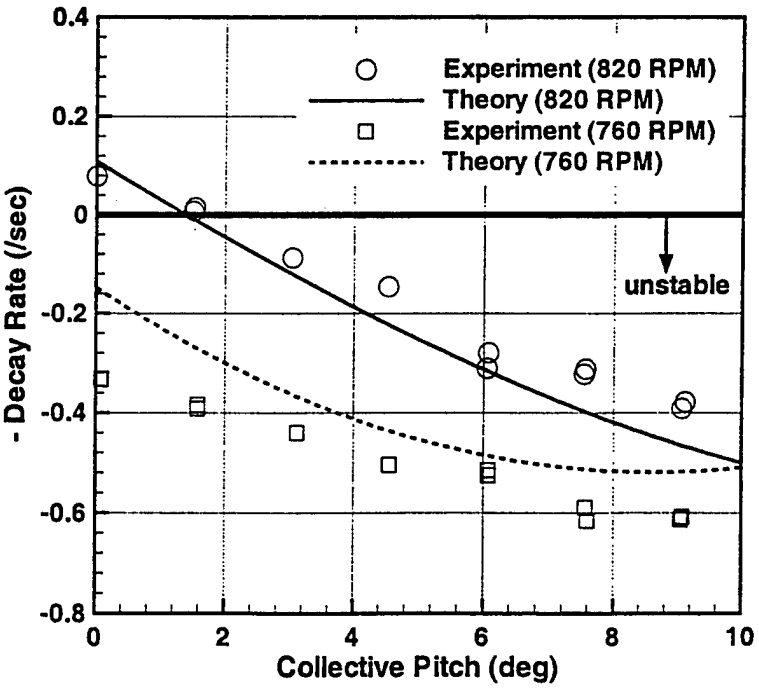

Fig 4: Variation of regressing lag damping vs. collective at 760 and 820 RPM

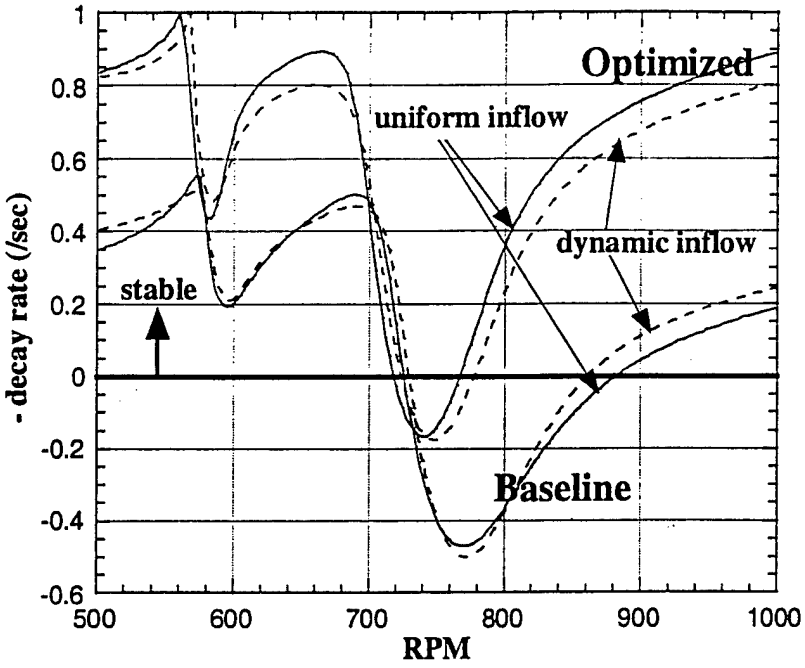

Fig 5: Dynamic vs. steady inflow (Coll. Pitch = 5°)

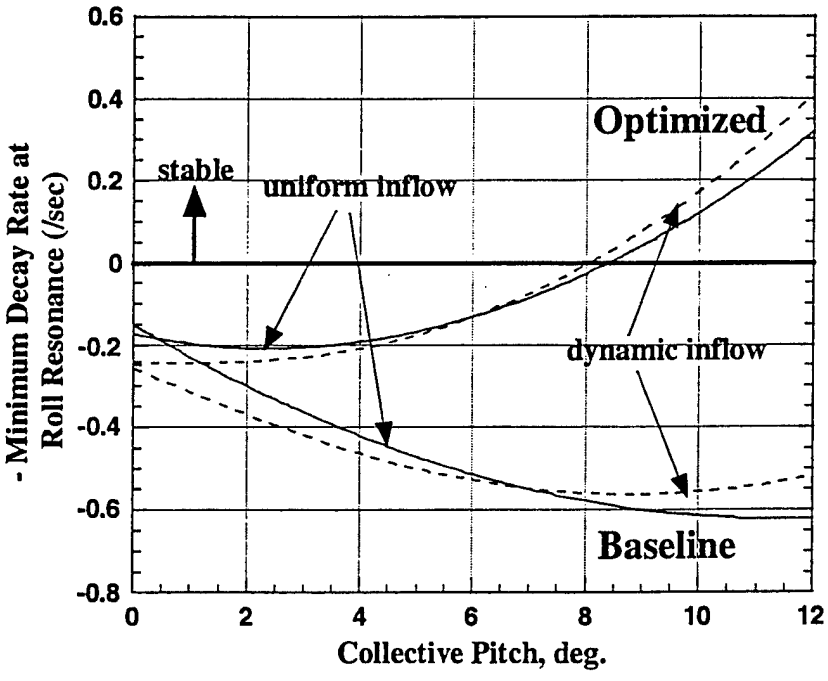

Fig 6: Dynamic vs. steady inflow: minimum lag mode stability vs. collective pitch

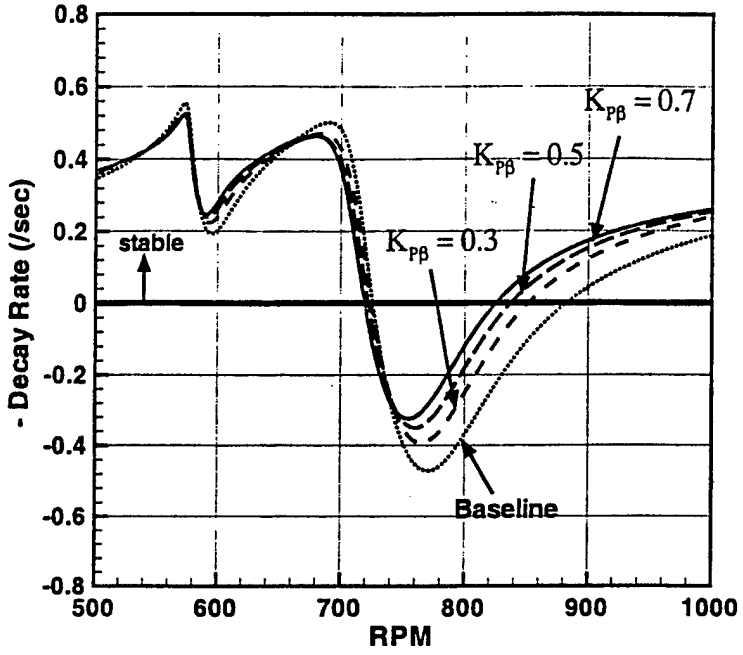

Fig 7: Influence of pitch-flap coupling on lag damping (5° collective pitch)

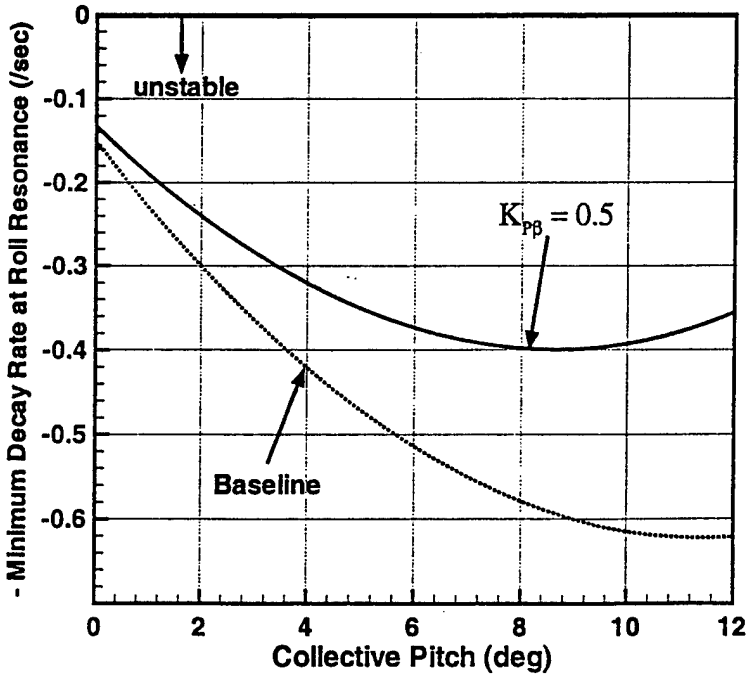

Fig 8: Influence of pitch-flap coupling on lag damping - variation of minimum damping vs collective pitch

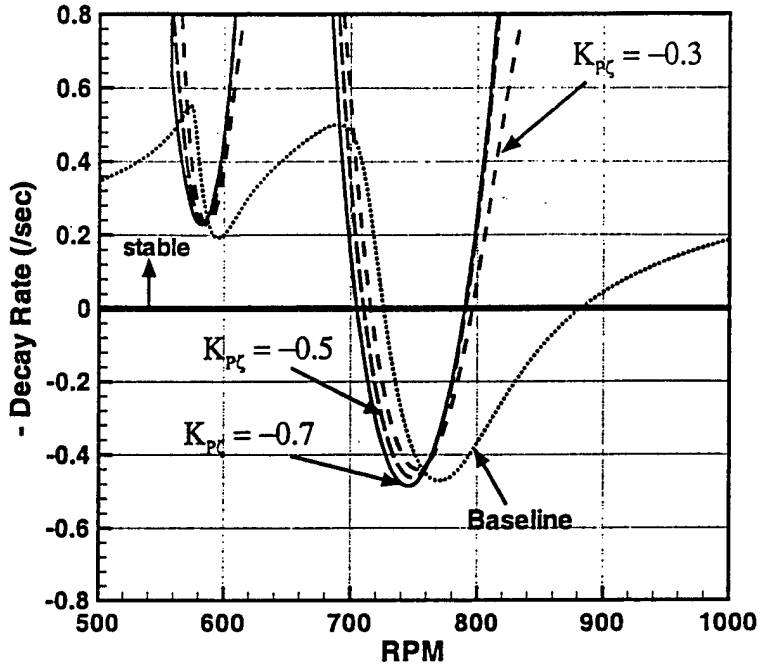

Fig 9: Influence of pitch-lag coupling on lag damping (5° collective pitch)

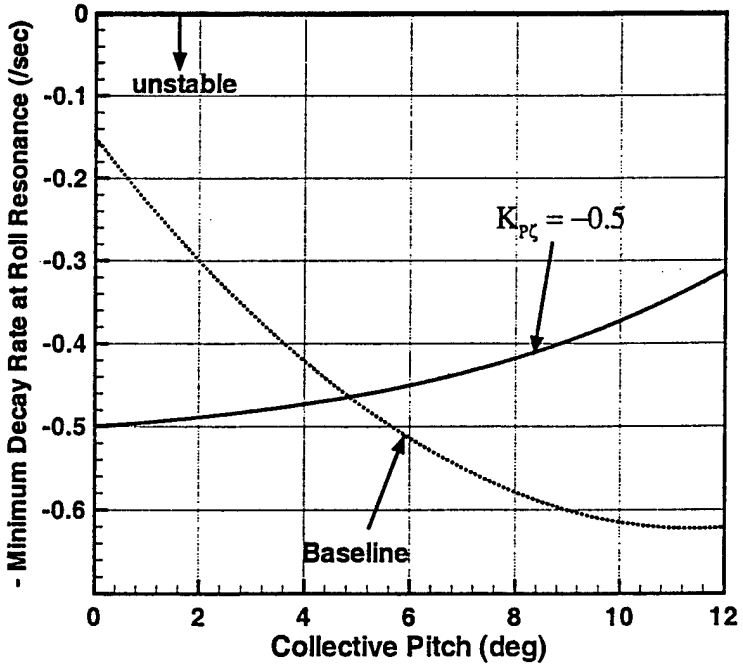

Fig 10: Influence of pitch-lag coupling on lag damping - variation of minimum damping vs collective pitch

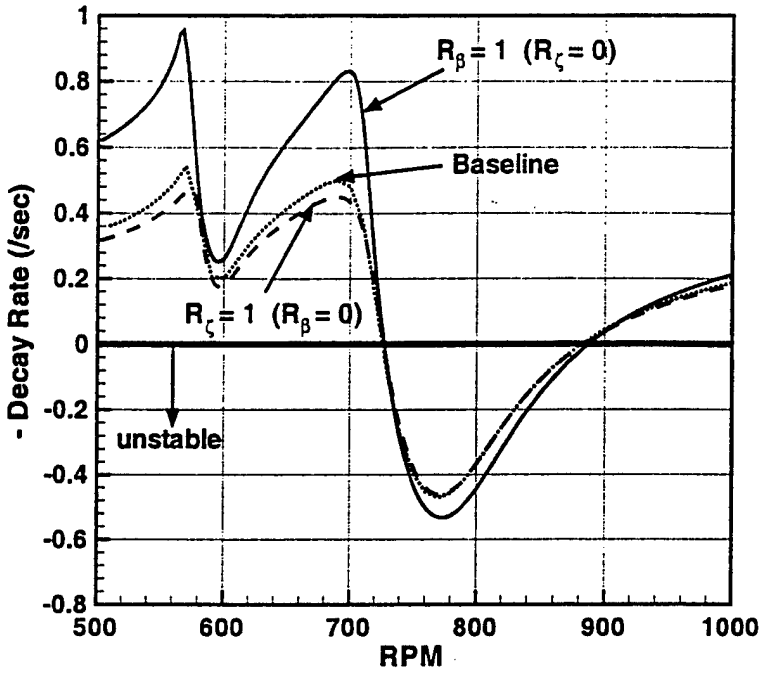

Fig 11: Influence of flap-lag coupling on lag damping (5° collective pitch)

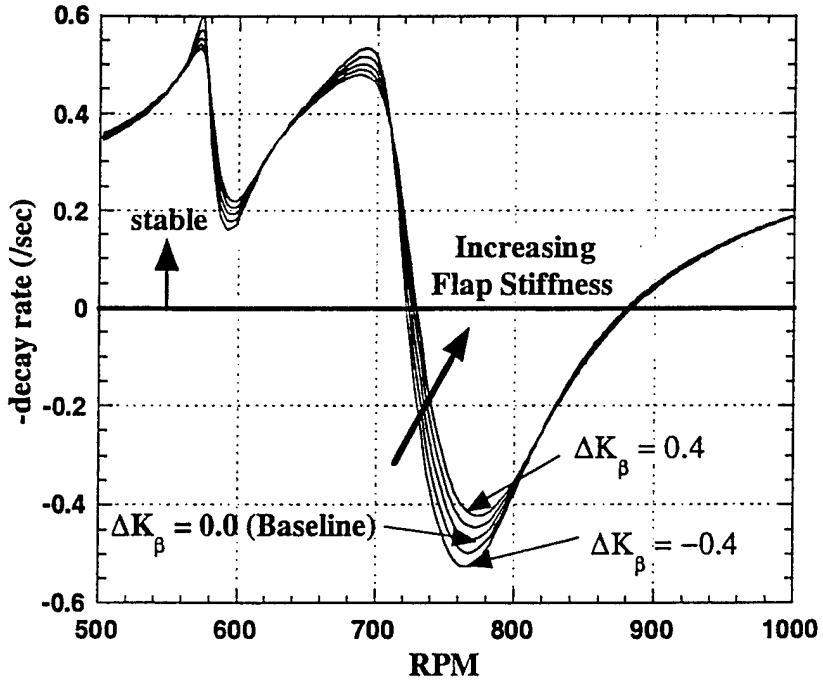

Fig 12: Influence of flap stiffness on lag mode stability (Coll. Pitch = 5°)

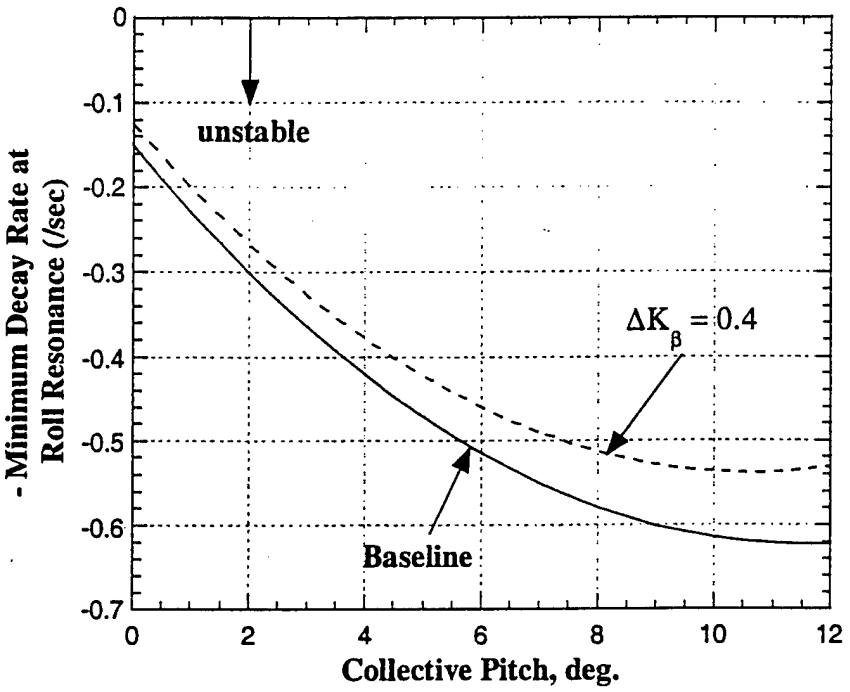

Fig 13: Influence of flap stiffness on lag mode stability – variation of minimum damping vs. collective pitch

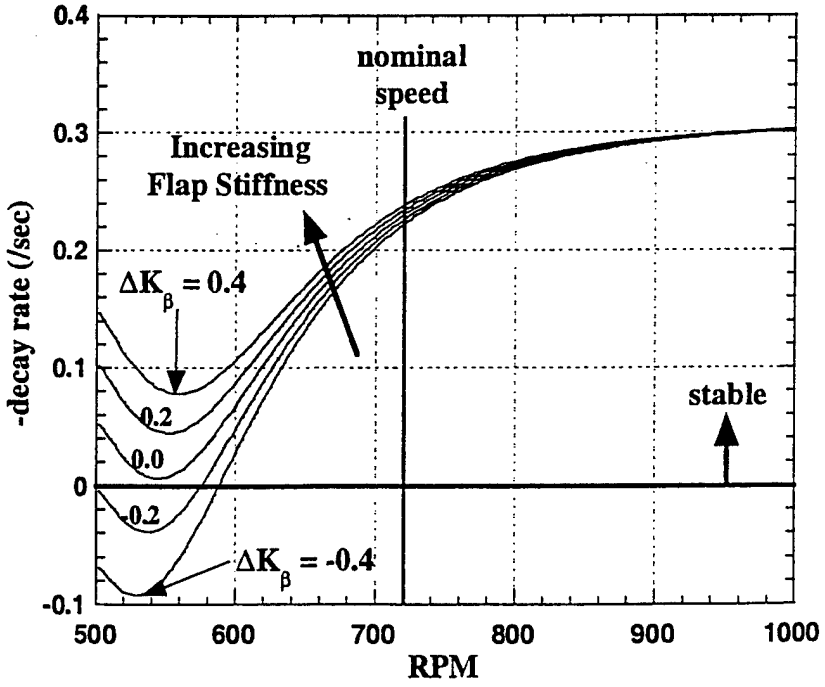

Fig 14: Influence of flap stiffness on lag mode stability – air resonance stability (nominal $C_T/\sigma = 0.07$)

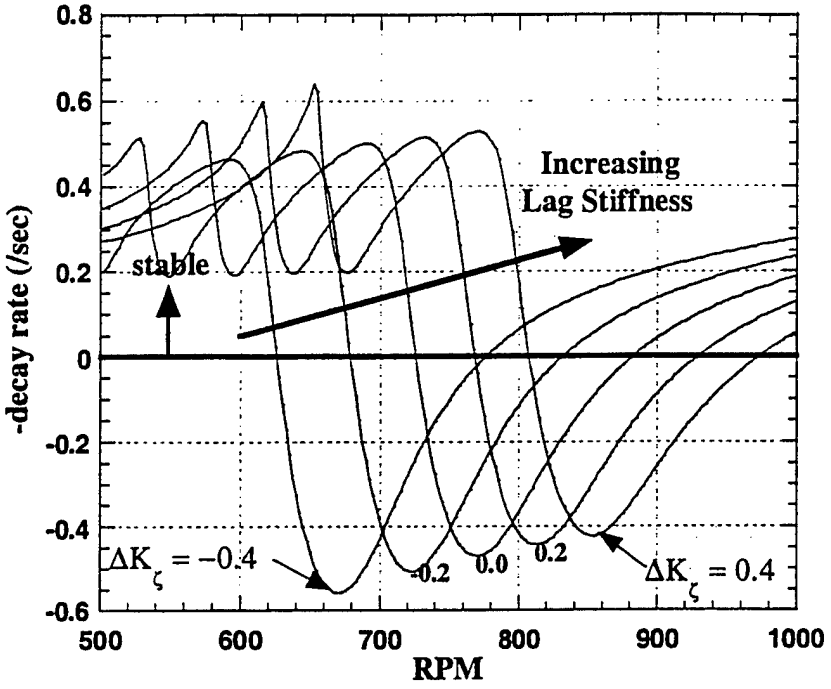

Fig 15: Influence of lag stiffness on lag mode stability (Coll. Pitch = 5°)

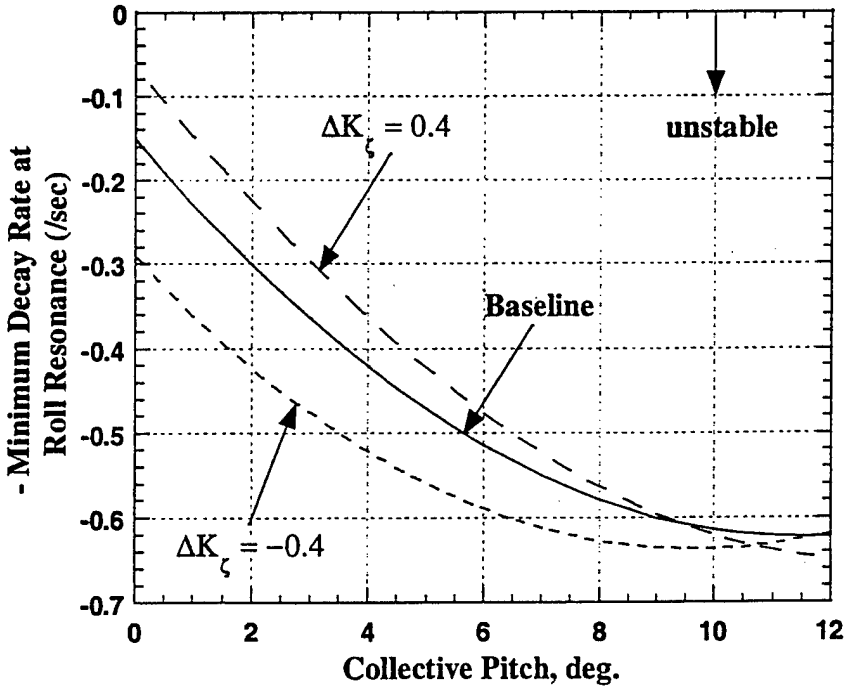

Fig 16: Influence of lag stiffness on lag mode stability – variation of minimum damping vs. collective pitch

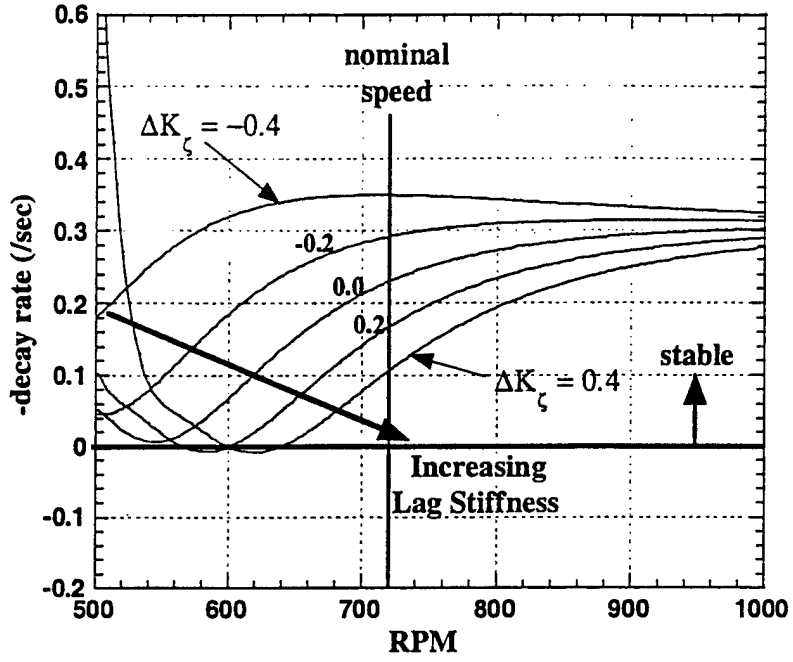

Fig 17: Influence of lag stiffness on lag mode stability – air resonance stability (nominal C_T/σ = 0.07)

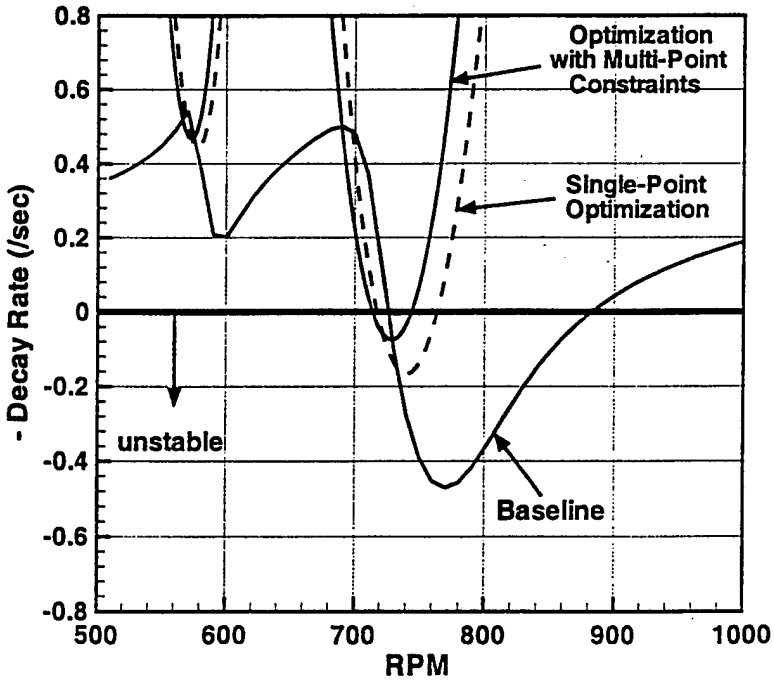

Fig 18: Influence of couplings obtained using single-point optimization on lag damping (5° collective pitch)

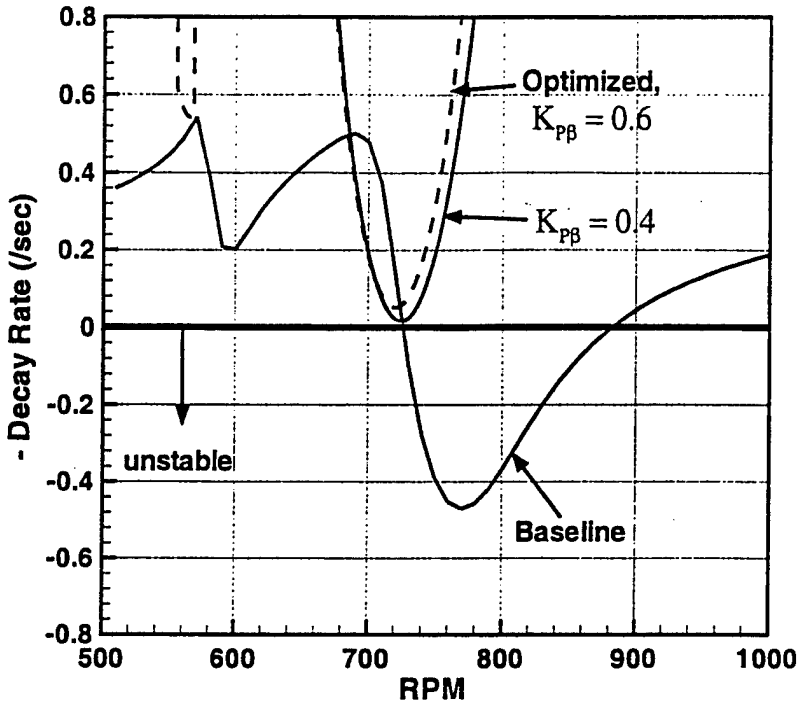

Fig 19: Influence of couplings obtained using moving-point optimization at 5° on lag damping (5° collective pitch)

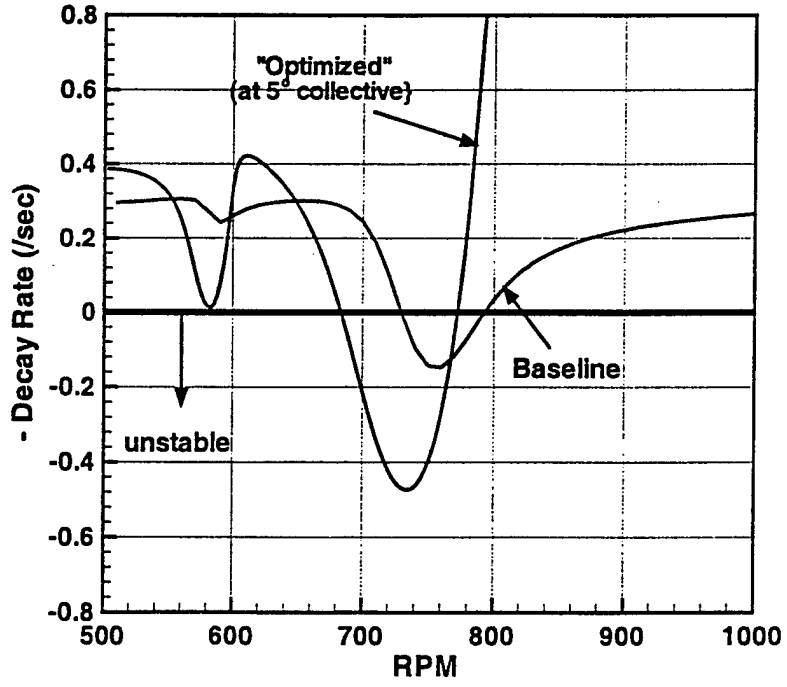

Fig 20: Influence of couplings obtained using moving-point optimization at 5° on lag damping (0° collective pitch)

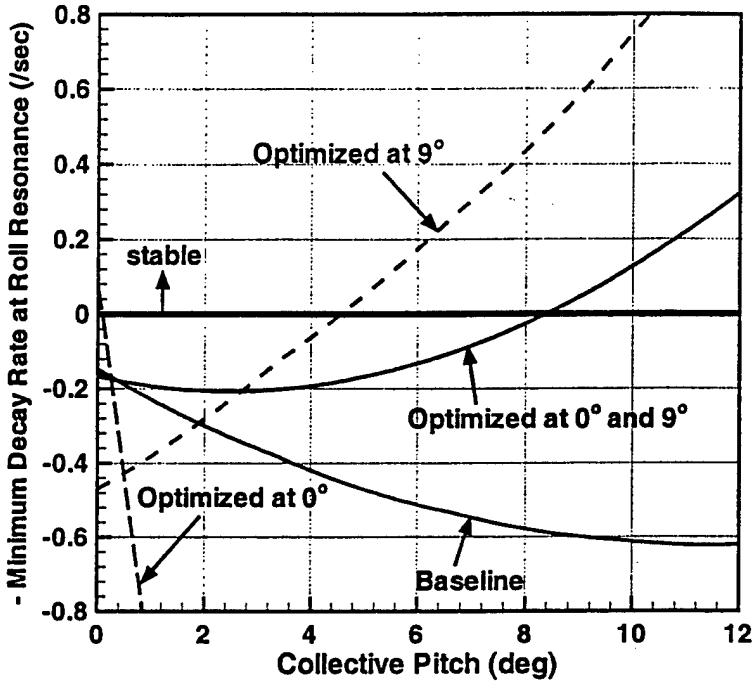

Fig 21: Variation of minimum damping vs collective pitch using different optimization schemes

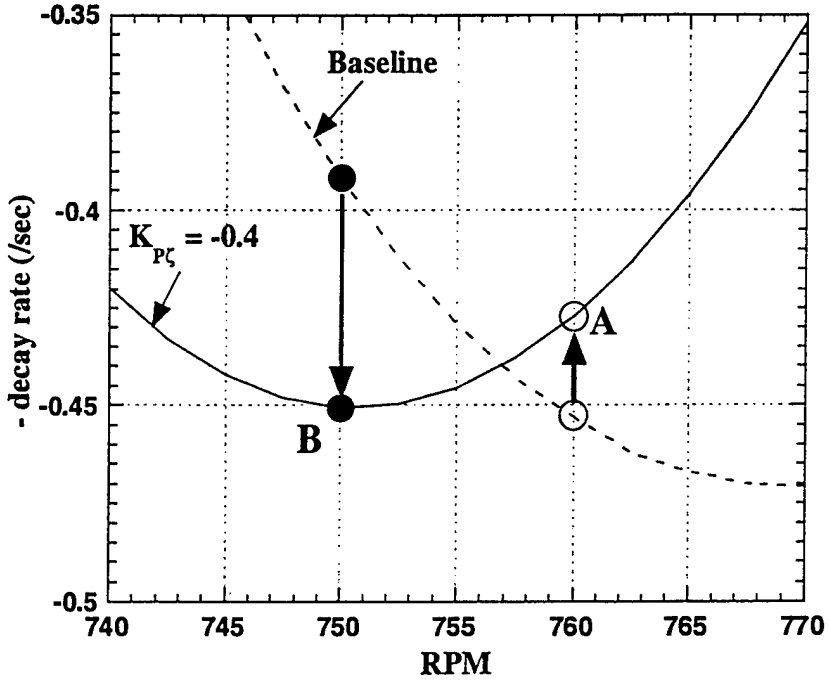

Fig 22: Illustration of discretization error in optimization process

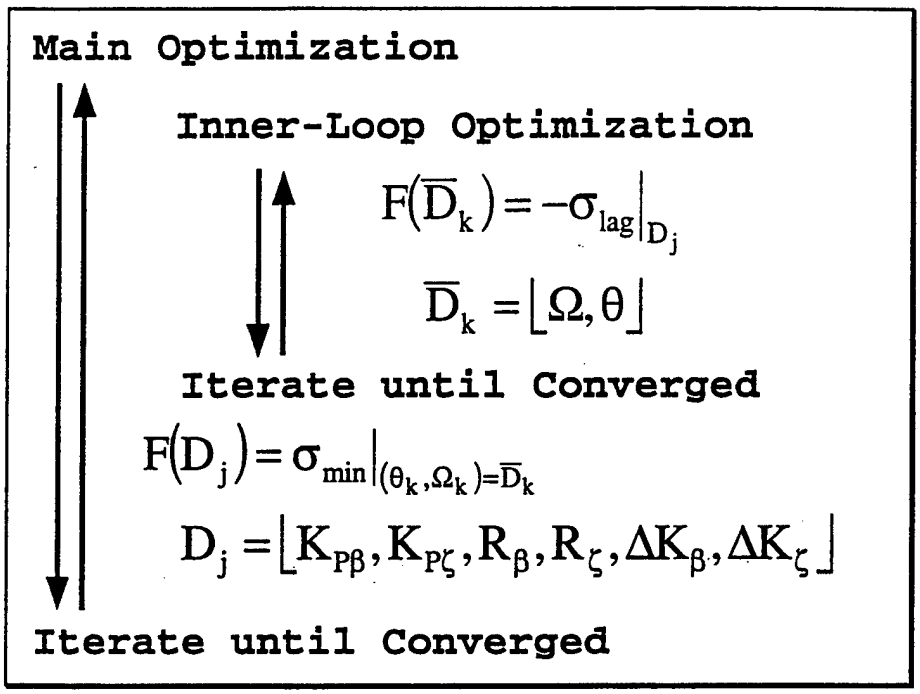

Fig 23: Outline of "two-stage" optimization process

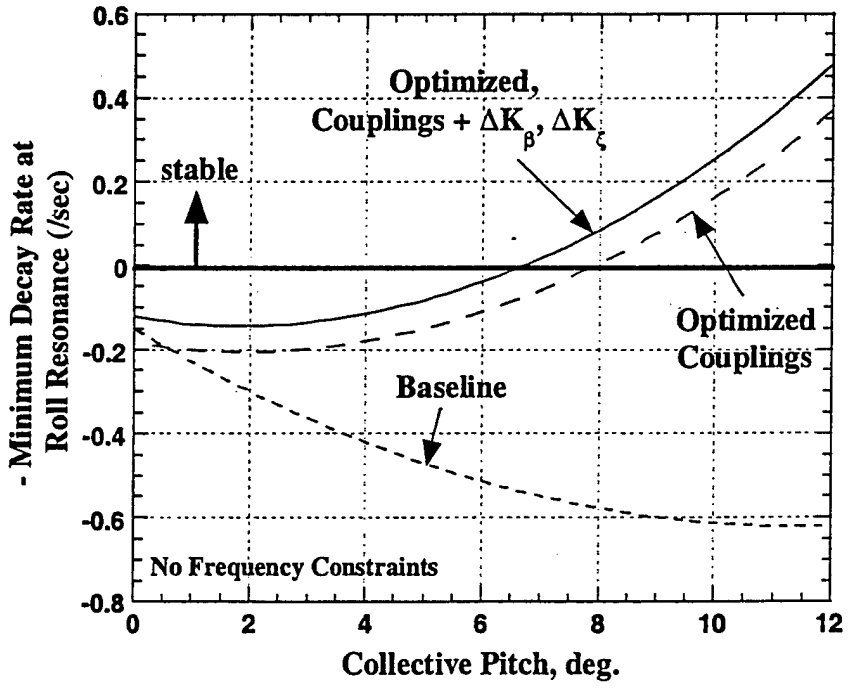

Fig 24: Variation of minimum damping versus collective pitch, comparison of optimized results without frequency constraints with baseline results

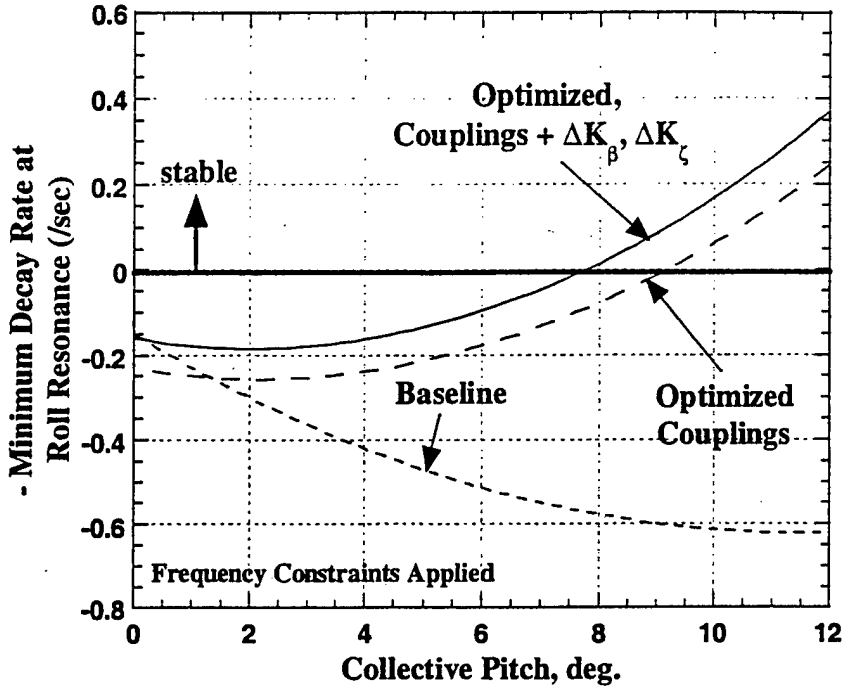

Fig 25: Variation of minimum damping versus collective pitch, comparison of optimized results with frequency constraints with baseline results

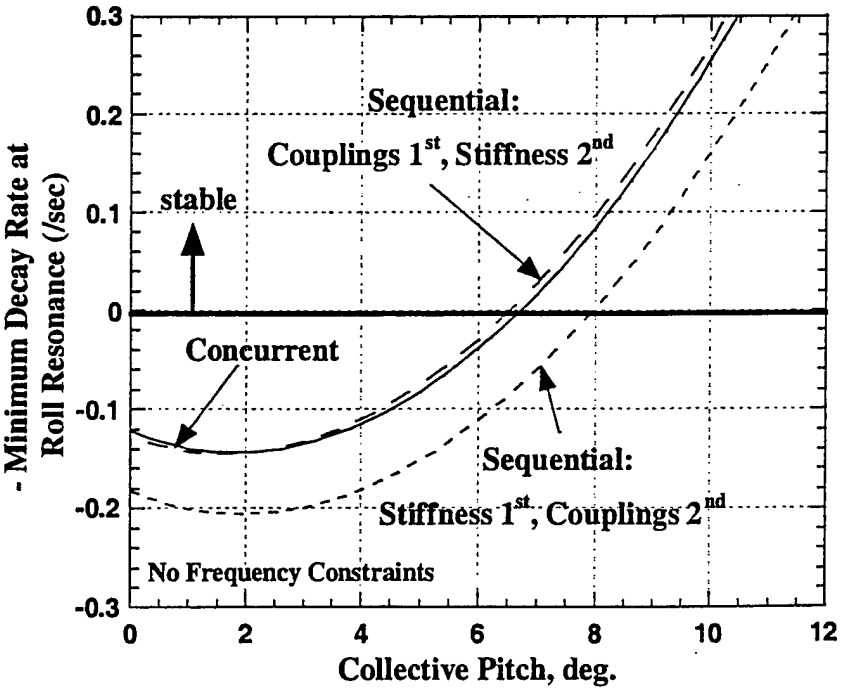

Fig 26: Variation of minimum damping versus collective pitch, sequential versus concurrent optimization techniques – no frequency constraints

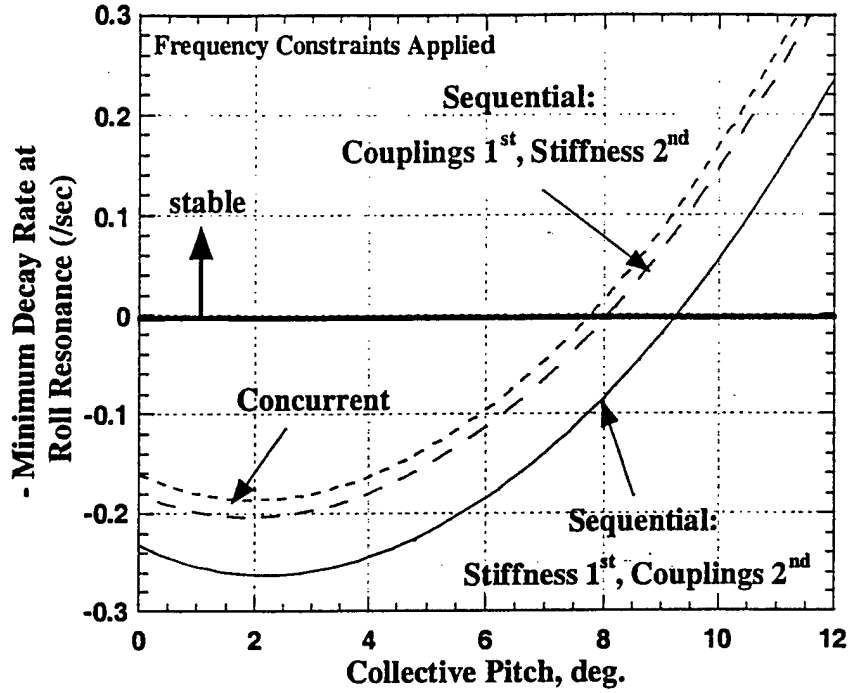

Fig 27: Variation of minimum damping versus collective pitch, sequential versus concurrent optimization techniques – frequency constraints active

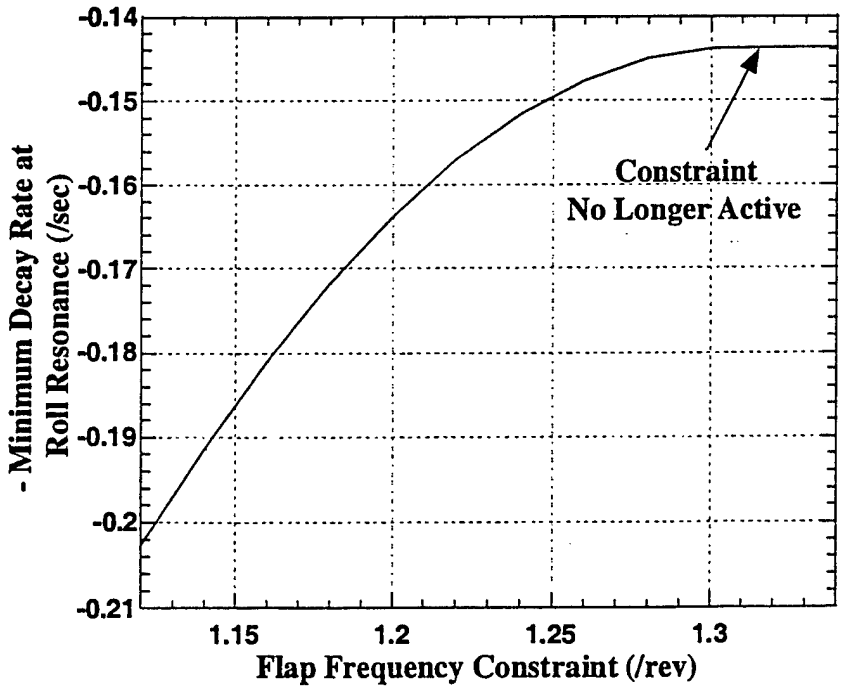

Fig 28: Variation of minimum damping as flap frequency constraint is relaxed

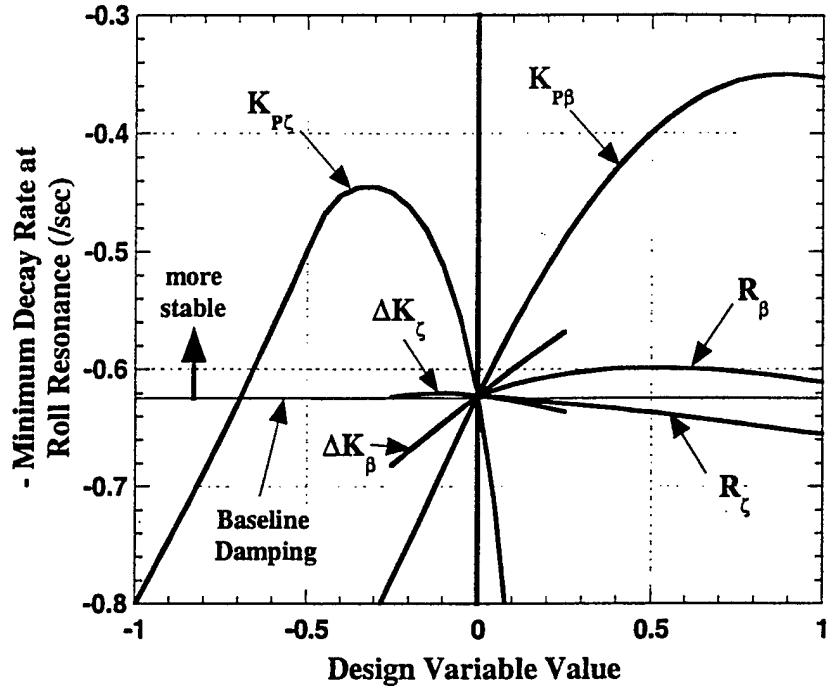

Fig 29: Variation of minimum damping with changes in design variables at the point of minimum damping - baseline configuration

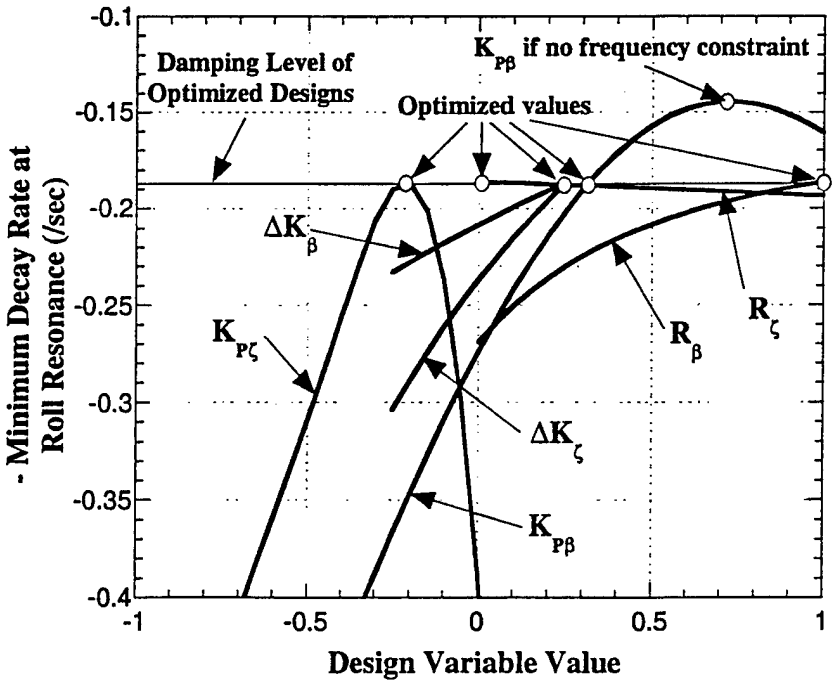

Fig 30: Variation of minimum damping with changes in design variables at the point of minimum damping - optimized configuration (Eq. 15)

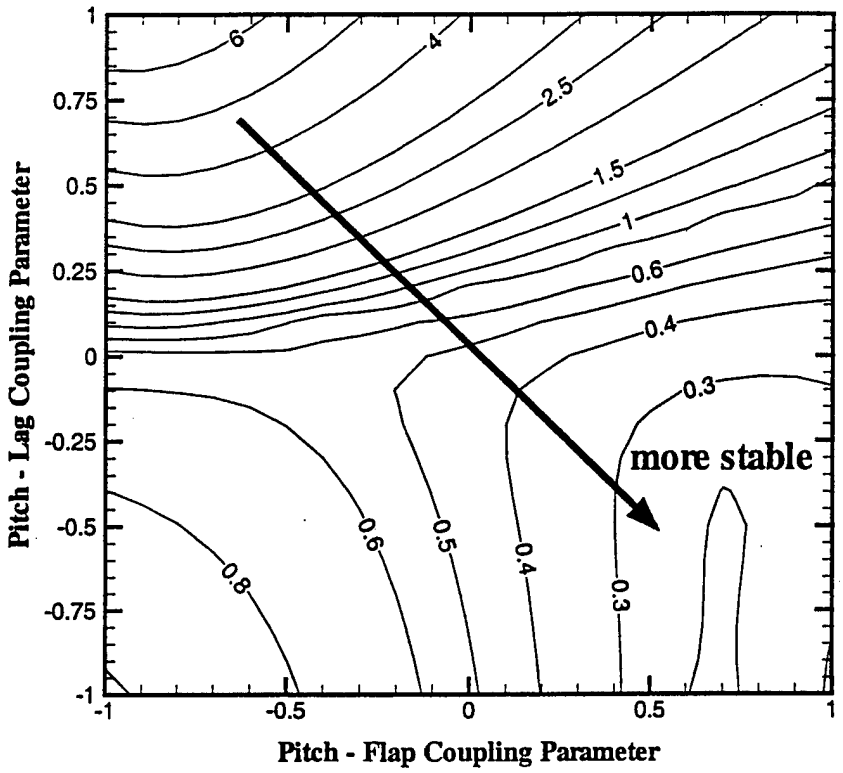

Fig 31: Contour plot - Variation of decay rate with pitch-flap and pitch-lag coupling (Coll. Pitch = 5°)

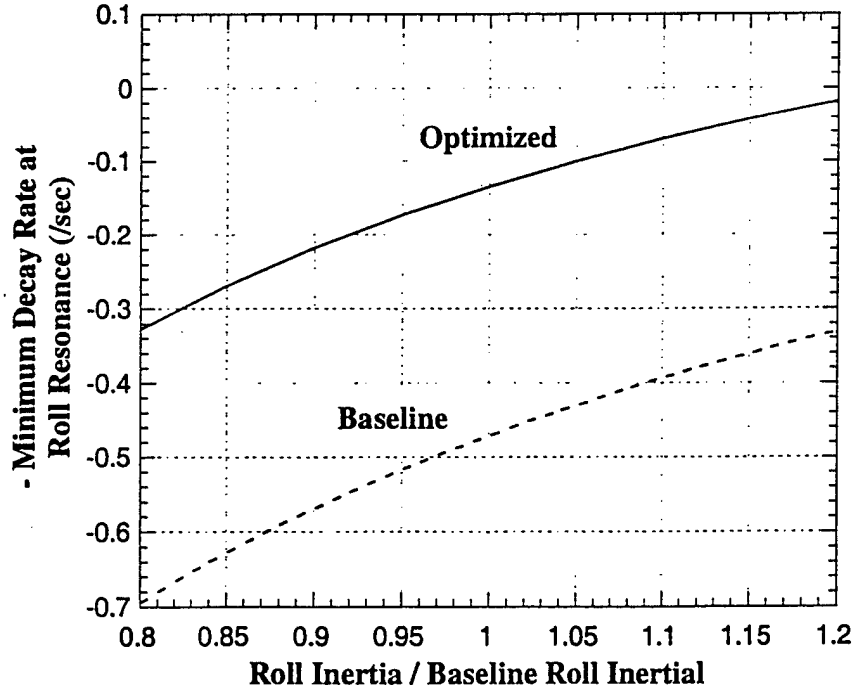

Fig 32: Variation of minimum damping versus roll inertia (Coll. Pitch = 5°)

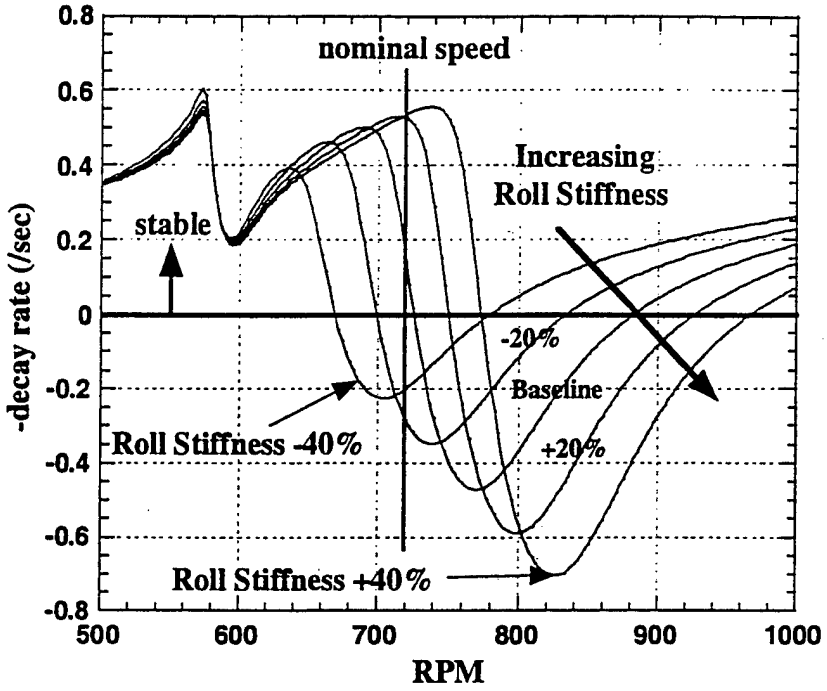

Fig 33: Influence of roll stiffness on lag mode stability – baseline configuration (Coll. Pitch = 5°)

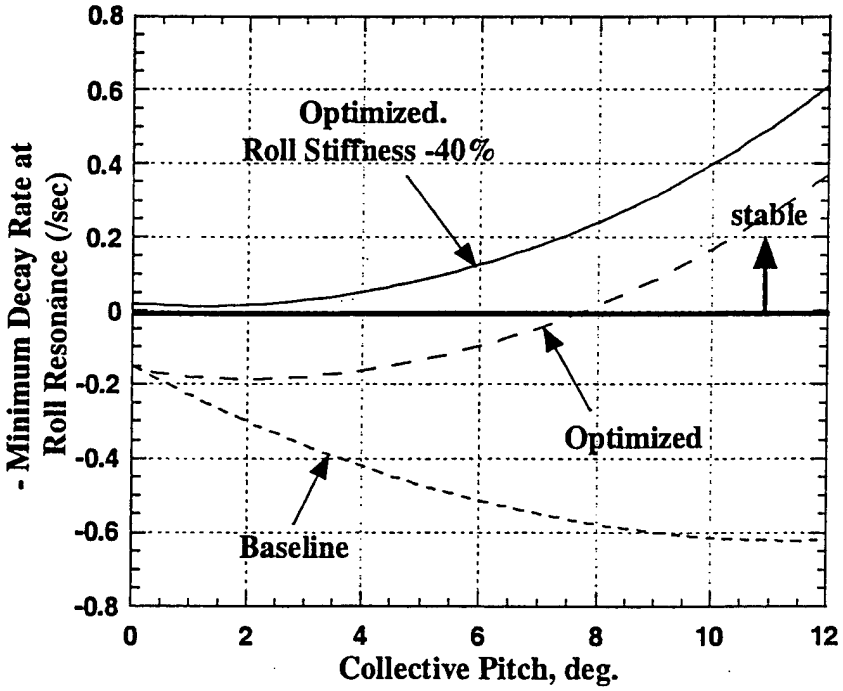

Fig 34: Influence of reduced roll stiffness on optimized results

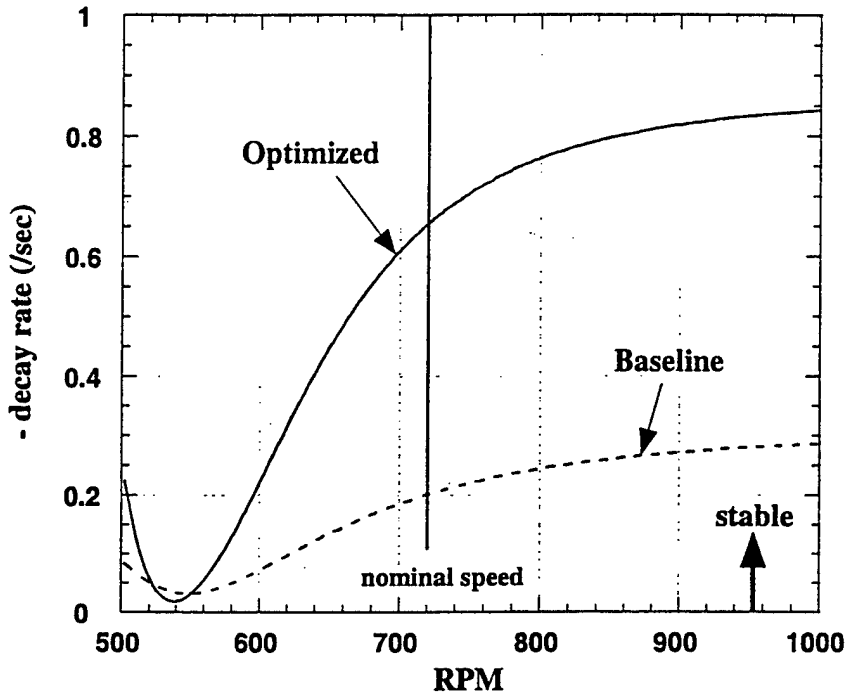

Fig 35: Influence of optimized configuration on air resonance stability in hover

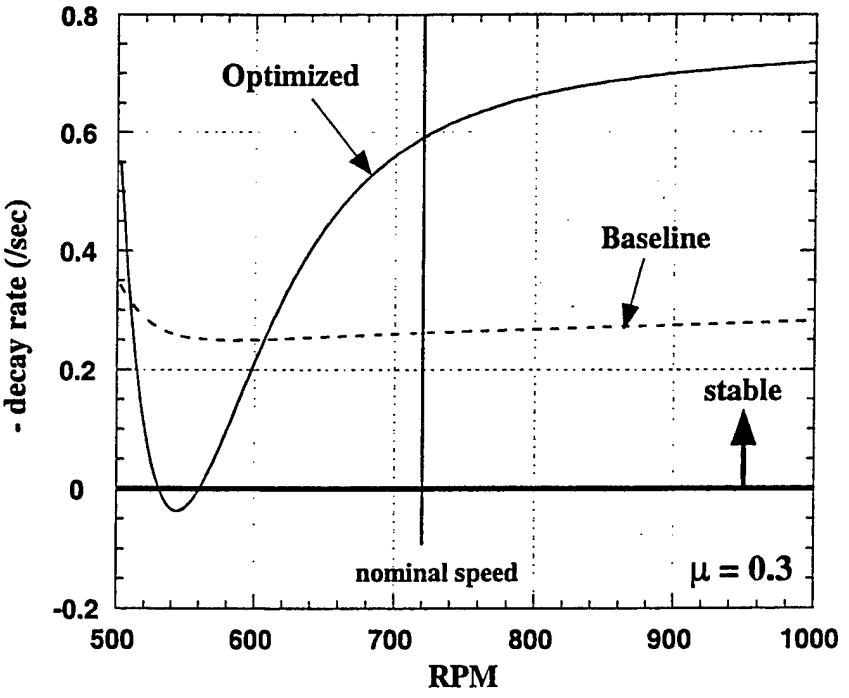

Fig 36: Influence of optimized configuration on air resonance stability in forward flight ($\mu = 0.3$)

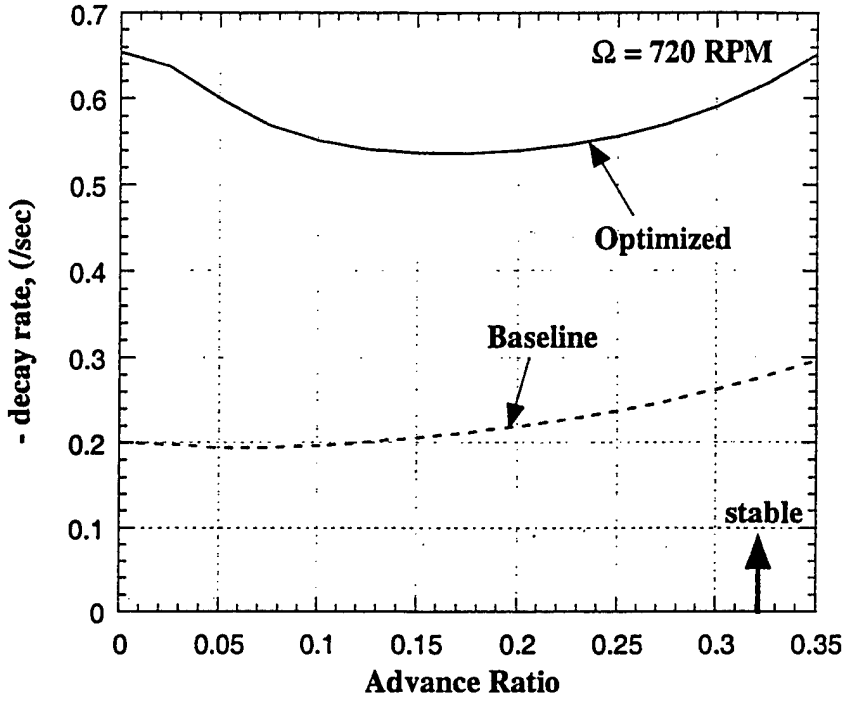

Fig 37: Variation of minimum damping versus advance ratio, baseline and optimized configuration

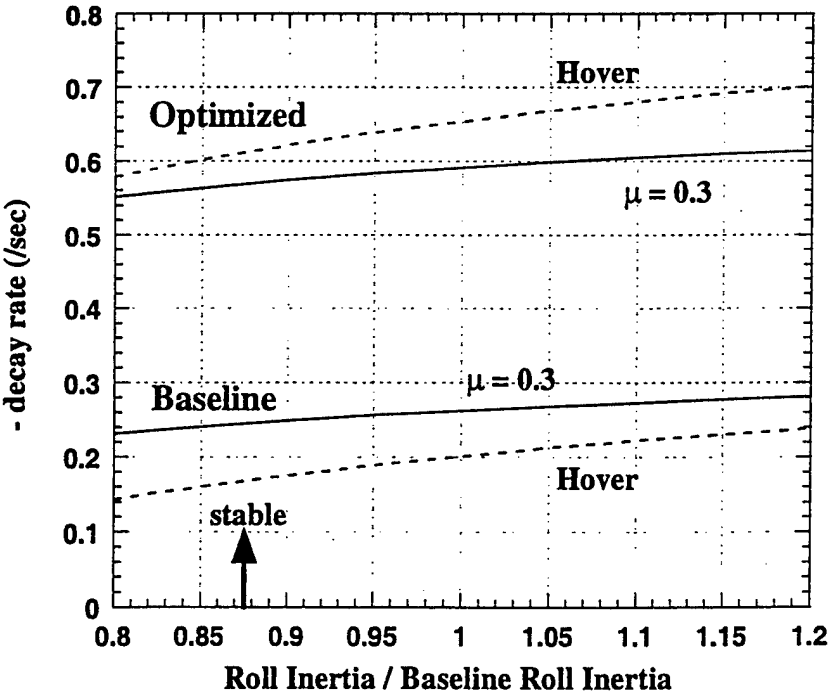

Fig 38: Variation of minimum damping versus roll inertia - air resonance stability